University of Alberta

Hydraulics of a Three Obstacle Cluster in Open Channels

by

Cory David Albers

A thesis submitted to the Faculty of Graduate Studies and Research

in partial fulfillment of the requirements for the degree of Master of Science

in

Water Resources Engineering

Department of Civil and Environmental Engineering

Edmonton, Alberta

Spring 1997

National Library of Canada
Acquisitions and Bibliographic Services
395 Wellington Street
Ottawa ON K1A 0N4
Canada

Bibliothèque nationale du Canada
Acquisitions et services bibliographiques
395, rue Wellington
Ottawa ON K1A 0N4
Canada

Your file Votre référence

Our file Notre référence

The author has granted a non-exclusive licence allowing the National Library of Canada to reproduce, loan, distribute or sell copies of his/her thesis by any means and in any form or format, making this thesis available to interested persons.

The author retains ownership of the copyright in his/her thesis. Neither the thesis nor substantial extracts from it may be printed or otherwise reproduced with the author's permission.

L'auteur a accordé une licence non exclusive permettant à la Bibliothèque nationale du Canada de reproduire, prêter, distribuer ou vendre des copies de sa thèse de quelque manière et sous quelque forme que ce soit pour mettre des exemplaires de cette thèse à la disposition des personnes intéressées.

L'auteur conserve la propriété du droit d'auteur qui protège sa thèse. Ni la thèse ni des extraits substantiels de celle-ci ne doivent être imprimés ou autrement reproduits sans son autorisation.

0-612-21149-5

Canada

University of Alberta

Library Release Form

Name of Author: Cory David Albers

Title of Thesis: Hydraulics of a Three Obstacle Cluster in Open Channels

Degree: Master of Science

Year this Degree Granted: 1997

Permission is hereby granted to the University of Alberta Library to reproduce single copies of this thesis and to lend to sell such copies for private, scholarly or scientific research purposes only.

The author reserves all other publications and other rights in association with the copyright in the thesis, and except as hereinbefore provided, neither the thesis nor any substantial portion thereof may be printed or otherwise reproduced in any material form whatever without the author's prior written permission.

19 Bradburn Crescent
St. Albert, Alberta
T8N 2J8

Date JAN 3, 1997

University of Alberta

Faculty of Graduate Studies and Research

The undersigned certify that they have read, and recommended to the Faculty of Graduate Studies and Research for acceptance, a thesis entitled Hydraulics of a Three Obstacle Cluster in Open Channels submitted by Cory David Albers in partial fulfillment of the requirements for the degree of Master of Science in Water Resources Engineering

Dr. N. Rajaratnam

Dr. P. Steffler

Dr. J. Leonard

Date 23 Dec 96

ABSTRACT

This thesis presents the results of an experimental study of flow around a three obstacle cluster in open channels. The dependence of the flow patterns on the depth of flow and the obstacle spacing were examined on a rigid bed. This was done through examination of the separation line from the bed near each obstacle and by observing the direction of the bed shear vector over a large area around the cluster. The cluster was found to act as a single obstacle to the flow when the center to center spacing was 1.1 obstacle diameters or less. Under this spacing condition a single horseshoe vortex forms around the obstacle cluster. This behavior was confirmed when the cluster of obstacles was placed on a mobile bed material and a scour hole was created around the cluster and not between the obstacles. The results of this study were used to present recommendations for design of fish habitat structures.

ACKNOWLEDGEMENTS

I wish to extend my sincere thanks to my supervisor, Dr. N. Rajaratnam who provided thoughtful advise and encouragement throughout my program. Dr. Rajaratnam's enthusiasm for his work and his belief in my abilities have been an inspiration to me in setting my career goals.

I am thankful for the financial support from the Department of Fisheries and Oceans, Government of Canada and to Chris Katopodis.

Thank you to Sheldon Lovell, Specialist Technician, at the T. Blench Hydraulics Laboratory for his advise and assistance with the experimental setup.

Thanks are due to my family for their consistently strong support. Thanks to my mother for her advise on manuscript organization. Thanks to my wife for her encouragement throughout my program.

Thank you to all my professors and colleagues in the Water Resources Group at the University of Alberta for providing a strong atmosphere of sharing and support. Thanks in particular to Dr. Hamid Shamloo for his advise and conversations regarding this work. Thanks also to Dr. Peter Steffler whose elementary course in Fluid Mechanics during my undergraduate degree first interested me in Water Resources.

TABLE OF CONTENTS

	Page
CHAPTER 1: INTRODUCTION	1
1.1 Statement of the Problem	1
1.2 Purpose and Scope of the Study	1
CHAPTER 2: GENERAL THEORY AND REVIEW OF LITERATURE	3
2.1 Introduction	3
2.2 Single Obstacles Fixed to a Rigid Wall	3
2.2.1 Horseshoe Vortices	3
2.2.2 Vortex Shedding	6
2.2.3 Arch Vortices	7
2.2.4 Single Hemisphere in Open Channel Flow	7
2.3 Considerations Associated with a Mobile Bed	8
2.3.1 Single Hemisphere in Open Channel Flow	8
2.3.2 Obstacle Groups	9
CHAPTER 3: EXPERIMENTAL SETUP AND TESTING PROGRAM	11
3.1 Laboratory Facilities	11
3.2 Model Criterion	11
3.2.1 Prototype River Characteristics	11
3.2.2 Model Froude Number	12
3.2.3 Obstacle Geometry and Placement	13
3.3 Data Collection	14
3.3.1 Flow Visualization	14
3.3.2 Capturing an Image from a Videotape	15
3.3.3 Data Extracted from Images	15
3.4 Testing Program	15

CHAPTER 4: EXPERIMENTAL RESULTS 20
4.1 Local Effects of the Cluster on a Rigid Bed 20
4.1.1 Separation Profile 20
4.1.2 Horseshoe Vortex Systems 21
4.1.2.1 LE Horseshoe Vortex Cascade, D = 5 cm and d/h = 0.5 21
4.1.2.2 LE Horseshoe Vortex, Other than D = 5 cm and d/h = 0.5 22
4.1.2.3 TE Horseshoe Vortex 23
4.1.3 Arch Vortex 24
4.1.4 Flow Separation Behind Obstacles 24
4.2 Extended Flow Effects of the Cluster on a Rigid Bed 25
4.2.1 Bed Shear Profile 25
4.2.2 Wake of the Obstacle Clusters 26
4.3 Effects of a Cluster on a Mobile Bed 26

CHAPTER 5: DISCUSSION 47
5.1 Major Findings 47
5.1.1 Depth of Flow 47
5.1.1.1 Bed Shear Profile Images 47
5.1.1.2 Separation Profile Images 48
5.1.1.3 Separation Profile Plots 48
5.1.1.4 Wake of Obstacles 49
5.1.2 Obstacle Spacing 50
5.1.2.1 Separation Profile Images 50
5.1.2.2 Bed Shear Profile Images 51
5.1.2.3 Separation Profile Plots 51
5.1.3 Obstacle Size 52

5.1.4 Mobile Bed Material 53
5.2 Limitations of the Study 54

CHAPTER 6: CONCLUSIONS AND RECOMMENDATIONS 55
6.1 Conclusions 55
6.1.1 Depth of Flow 55
6.1.2 Obstacle Spacing 56
6.1.3 Obstacle Size 56
6.1.4 Mobile Bed Material 57
6.2 Recommendations 57
6.2.1 Designs for Fish Habitat Structures 57
6.2.2 Future Research 58

REFERENCES 59

APPENDIX A 61

APPENDIX B 66

LIST OF TABLES

Page

Table 3.1 Experimental testing program 17

LIST OF FIGURES

		Page
Figure 2.1	Fluid movement and vorticity orientation for the horseshoe vortex	10
Figure 2.2	Wind tunnel vortex cascade (Adapted from Baker - 1980)	10
Figure 3.1	Experimental setup	18
Figure 3.2	Plan view of obstacle geometry	19
Figure 4.1	Separation profile length scales	28
Figure 4.2	Normalized length scale "a/D" as a function of d/h	29
Figure 4.3	Normalized length scale "b/D" as a function of d/h	29
Figure 4.4	Normalized length scale "c/D" as a function of d/h	30
Figure 4.5	Normalized length scale "e/D" as a function of d/h	30
Figure 4.6	Normalized length scale "f/D" as a function of d/h	31
Figure 4.7	Normalized length scale "a/D" as a function of the spacing parameter S	31
Figure 4.8	Normalized length scale "b/D" as a function of the spacing parameter S	32
Figure 4.9	Normalized length scale "c/D" as a function of the spacing parameter S	32
Figure 4.10	Normalized length scale "e/D" as a function of the spacing parameter S	33
Figure 4.11	Normalized length scale "f/D" as a function of the spacing parameter S	33
Figure 4.12	Normalized length scale "a/D" as a function of d/4 (Including RS5-S/S', d=1.2 cm	34
Figure 4.13	Normalized length scale "b/D" as a function of d/h (Including RS5-S/S', d=1.2 cm)	34
Figure 4.14	Normalized length scale "e/D" as a function of d/h (Including RS5-S/S', d=1.2 cm)	35
Figure 4.15	Normalized length scale "f/D" as a function of d/h (Including RS5-S/S', d=1.2 cm)	35
Figure 4.16	Normalized length scale "a/D" as a function of the spacing parameter S (Including RS5-S/S', d=1.2 cm)	36
Figure 4.17	Normalized length scale "b/D" as a function of the spacing parameter S (Including RS5-S/S', d=1.2 cm)	36
Figure 4.18	Normalized length scale "e/D" as a function of the spacing parameter S (Including RS5-S/S', d=1.2 cm)	37

Figure 4.19 Normalized length scale "f/D" as a function of the spacing parameter S (Including RS5-S/S', d=1.2 cm) 37
Figure 4.20 Horseshoe vortex cascade - side view 38
Figure 4.21 Horseshoe vortex cascade - plan view 39
Figure 4.22 LE vortex filaments deflected between TEs 40
Figure 4.23 Arch vortex shedding from LE when S/S' ≥ 1.7/1.8 41
Figure 4.24 Arch vortex shedding from LE when S/S' < 1.7/1.8 41
Figure 4.25 Schematic of arch vortex shedding from LE when S/S' < 1.7/1.8 42
Figure 4.26 Vortex systems between TEs producing a surface boil 42
Figure 4.27 Fluid separation behind LE with small spacing 43
Figure 4.28 Asymmetrical vortex shedding 44
Figure 4.29 Symmetrical vortex shedding from the obstacle cluster 45
Figure 4.30 Independent obstacle wakes 46
Figure 4.31 Movement of cluster placed on a mobile bed 46
Figure A1 Composite SP, D = 5 cm, 1.3/1.4 ≥ S/S' ≥ 1.0/1.0 61
Figure A2 Composite SP, D = 5 cm, 1.8/2.0 ≥ S/S' ≥ 1.4/1.6 62
Figure A3 Composite SP, D = 5 cm, d≥h 63
Figure A4 Composite SP, D = 10 cm 64
Figure A5 Composite SP, D = 8.2 cm 65
Figure B1 Composite BSP, D = 10 cm, S/S' = 1.0/1.0 66
Figure B2 Composite BSP, D = 10 cm, S/S' = 1.1/1.2 67
Figure B3 Composite BSP, D = 10 cm, S/S' = 1.3/1.4 68
Figure B4 Composite BSP, D = 10 cm, S/S' = 1.4/1.6 69
Figure B5 Composite BSP, D = 10 cm, S/S' = 1.7/1.8 70
Figure B6 Composite BSP, D = 10 cm, S/S' = 1.8/2.0 71
Figure B7 Composite BSP, D = 5 cm, S/S' = 1.0/1.0 72
Figure B8 Composite BSP, D = 5 cm, S/S' = 1.1/1.2 73

Figure B9 Composite BSP, D = 5 cm, S/S' = 1.3/1.4 74
Figure B10 Composite BSP, D = 5 cm, S/S' = 1.4/1.6 75
Figure B11 Composite BSP, D = 5 cm, S/S' = 1.7/1.8 76
Figure B12 Composite BSP, D = 5 cm, S/S' = 1.8/2.0 77
Figure B13 Composite BSP, D = 8.2 cm, S/S' = 1.1/1.2 78
Figure B14 Composite BSP, D = 8.2 cm, S/S' = 1.4/1.6 79
Figure B15 Composite BSP, D = 8.2 cm, S/S' = 1.8/2.0 80

LIST OF SYMBOLS

Symbol	Description
a, b, c, e, f	Distances from obstacles to the separation line (L)
d	Depth of flow (L)
D	Obstacle Diameter (L)
D50	Mean Sand Grain Diameter (L)
Fr	Froude number
g	Gravitational acceleration (L/T^2)
h	Height of obstacle (L)
n	Frequency of vortex shedding (1/T)
R	Reynolds number
S	Scalar of D giving the center to center spacing of the LE to the TE
S'	Scalar of D giving the center to center spacing between the TEs
St	Strouhal number
V	Velocity of flow (L/T)
x, y, z	Orthogonal coordinates (L)
α, β	Streamline labeling symbols
δ^*	Displacement thickness of the boundary layer (L)
ν	Kinematic viscosity of water (L^2/T)
ξ_z	Vorticity in the z direction (1/T)

LIST OF ABREVIATIONS

Abreviation	Description
BSP	Bed Shear Profile
SP	Separation Profile
LE	Leading Element
TE	Trailing Element
HS	Horseshoe
RS	Rigid Smooth (indicator of bed configuration)
MR	Mobile Rough (indicator of bed configuration)

CHAPTER 1

INTRODUCTION

1.1 Statement of the Problem

Flow regimes in rivers are significantly influenced by human development. An example of this influence is the rapid and large changes in river discharge that are required to meet the demand of cyclical power production. Another example is highway construction beside rivers that significantly restrict the channel flow area. Unnatural influences like these can strip rivers of features such as boulders, or sunken logs. Changes of any kind to the flow regime of a river affects the fish living within.

It has recently become a legal requirement that developments permit "no net loss of fish habitat" (Department of Fisheries and Oceans, 1986) in rivers to occur due to a human presence. The problem for governments and industry is replacing natural habitat lost to development with a net equivalent artificial habitat. One of many solutions that is currently being used is to place a large rock in a habitat poor reach. For this solution to be effective requires that the condition of structure stability during high discharge and precise habitat hydraulics at low discharge be satisfied by a single design. Flood flows introduce enormous forces on obstacles which are supported by materials that are most mobile during the same flood event. Large rocks may be placed as artificial habitat however enormous rocks, which are more stable during high flow events, pose handling difficulties that make their general use impractical.

1.2 Purpose and Scope of the Study

The primary purpose of this study is to investigate the general flow structure around a three obstacle cluster fixed to a rigid smooth bed. It is hoped that a cluster of obstacles will produce conditions of enhanced stability for each individual obstacle while providing

similar hydraulic conditions associated with a single, much larger obstacle. Three parameters were independently varied in this study; obstacle size, obstacle spacing and depth of flow. Observations were made on the position of the bed separation line near each obstacle in the cluster and on the direction of the bed shear vector over an extended area around the cluster. Additional observations were made on the nature of the vortex systems around each obstacle and on the general characteristics of the wake behind the cluster or behind each obstacle. The results of this study will be used to verify or modify current guidelines for rock cluster fish habitat design in Alberta (Lowe, 1992).

The secondary purpose of this study is to investigate the movement, induced by flowing water, of obstacles placed on a mobile bed material. This portion of the study was restricted to a single test where the major movements of each obstacle in the cluster was documented. The results from this portion of the study will be used to make recommendations for future research involving multiple obstacles on a mobile bed.

CHAPTER 2

GENERAL THEORY AND REVIEW OF LITERATURE

2.1 Introduction

Many investigators have studied the behavior of obstacles exposed to flowing fluids. As with most problems in Fluid Mechanics, the complexity of natural problems require that significant simplifications be made before any basic understanding of the phenomenon can be reached. Studies conducted on three dimensional flows are relatively few and they borrow many concepts from studies of fluid behavior in two dimensions. Under special conditions, many problems can be reasonably reduced to a two dimensional problem. However many flows in nature do exhibit three dimensional flow behavior. Most classical studies are also limited in scope to focusing on flows around single obstacles instead of around obstacle groups.

2.2 Single Obstacles Fixed to a Rigid Wall

2.2.1 Horseshoe Vortices

One of the most notable vortices associated with obstacles to fluid flows is the horseshoe (HS) vortex. This vortex forms on the upstream side of an obstacle and develops into a high speed rotating fluid mass that can produce bed shear stresses that are many times larger than the free stream bed shear stress (Ahmed, 1994). The HS vortex is a generally stable flow feature. However, the precise position of the vortex in front of an obstacle oscillates in a complicated manner (Baker, 1979).

The HS vortex is a vortex that is not terminated at a rigid flow boundary but owes it's existence to the vorticity generated near the primary flow boundary. If we consider flow in the x-y plane (Figure 2.1) the definition of vorticity in the z direction (ξ_z) is (Potter and Wiggart, 1986):

$$\xi_z = \frac{\partial v}{\partial x} - \frac{\partial u}{\partial y} \qquad (2.1)$$

Similar equations exist describing vorticity in the x and y directions. The first term on the R. H. S. of Equation 2.1 dominates the equation since it is common to assume a uniform flow condition where only the gradient $\partial u/\partial y$ is considered nonzero.

The HS vortex represents a concentration of vorticity at the front of the obstacle. The viscous shearing associated with the presence of vorticity ensures that vorticity will diffuse over time and the energy of motion contained in the fluid decreases. This diffusion of vorticity is contrary to the ideal vortex where the strength of a vortex remains constant (Prandtl and Tietjens, 1957). For inertial flows, viscous diffusion of vorticity is a relatively slow process and vorticity may therefore accumulate to create a stable vortex. Since viscous dissipation of vorticity is a slow process in an inertial system, large concentrations of vorticity near obstacles must be permitted a transport mechanism away from the area of concentration. This transport mechanism manifests itself in the form of vortex filaments or shed vortices that are advected with the flow away from the obstacle. While stable, these vortex filaments are easily visualized by dye injected into the core since an ideal vortex is always composed of the same fluid elements (Prandtl and Tietjens, 1957).

Figure 2.1 illustrates the fluid movements (black arrows) within a control volume immediately upstream of the obstacle. Assuming there is no flow across the top boundary of the control volume, the bottom boundary or the boundary with the obstacle, the fluid that is transported into the front of the control volume must exit through the sides. The fluid transported into the control volume contains vorticity, a vector quantity,

with orientation (right hand rule) denoted by the dotted arrows. As the fluid is transported through the boundaries of the control volume vorticity is transported through the same boundaries. Upon entering the control volume the orientation of the vorticity vector is normal to streamwise and is distributed evenly over the surface of the wall. In front of the obstacle the fluid is decelerated and changes direction which permits the vorticity to concentrate. The fluid entering the control volume then curls into a large stable vortex. Fluid exiting the control volume flows parallel to the axis of the vorticity and is convected downstream on either side of the obstacle as free vortex filaments thus producing the characteristic HS shape.

Convection of vortex filaments may influence the behavior of vortex systems near downstream obstacles since the filaments represent a transportation of concentrated vorticity. The filaments may remain stable for 2-3 obstacle diameters downstream of the obstacle (Shamloo, 1997) and may influence other vortex systems before becoming unstable. At larger distances from the obstacle the turbulence in the ambient fluid distorts the filaments to the point of being unstable.

Wind tunnel tests on a cylinder fixed to a plane, rigid wall produce a series of HS vortices between the cylinder and the separation point of the primary flow from the wall. In this work by Baker (1980) there was observed a cascade with two primary vortices (vortex 1 and 2 in Figure 2.2) and two secondary vortices (vortex 0 and 1' in Figure 2.2). The primary vortices are larger, rotate faster, are further from the wall and directly capture fluid from the main flow. The minor vortices are located next to the wall, beneath the saddle point between the primary vortices. The circulation of the minor vortices, opposite to the primary vortices, is induced by viscous shear with the primary vortices. Considering the rotational direction of each vortex we can see that the bed shear stress will be away from the obstacle beneath the major vortices and towards the obstacle

beneath the minor vortices. Furthermore, one can see that the fluid entrained by the minor vortices must be transported to the system between the two streamlines defined by the stagnation streamline on the front of the obstacle and the outermost streamline that bounds vortex 1. In an earlier study, Baker (1979) found that the HS vortex systems oscillated such that "the frequency of these oscillations is solely determined by the values of VD/ν and δ*/D." where V is the free stream velocity, D is the obstacle diameter, ν is the kinematic viscosity of the fluid and δ* is the displacement thickness of the boundary layer. Okamoto (1977) described a vortex cascade in front of a cone where the vortex filaments from two primary HS vortices intertwined with each other to form what he termed 'necklace-vortices'.

2.2.2 Vortex Shedding

The original work on vortex shedding from cylinders by Strouhal and the later studies by von Karman were described by Rouse (1963). Vortices shed by cylinders are two dimensional in nature such that the axis of rotation is normal to the direction of fluid flow and parallel to the axis of the cylinder. The shedding is cyclical so that vortices are alternately shed from each side of the obstacle. The classical pattern of vortices behind the obstacles is known as a Karman Vortex Street. The frequency of vortex shedding (n), the diameter of the obstacle (D) to the flow and the approach velocity of the fluid (V) are all functionally related through the Strouhal number (St) where

$$St = \frac{nD}{V} \qquad (2.2)$$

The Strouhal number is in turn uniquely related to the Reynolds number (R) of the approaching flow. Von Karman's original treatment was based on a mathematical model where irrotational flow was assumed. This assumption of irrotational flow could not

have predicted the functional relationship between St and R since R is dependent on the viscosity of a fluid. It is only in an intermediate range of values for R that alternating vortices produce a vortex street. Very low values of R do not permit the fluid to separate from the obstacle at all. At sufficiently high values of R instabilities in the shedding vortices do not permit the oscillating series of vortices to develop and the wake becomes fully turbulent.

2.2.3 Arch Vortices

Okamoto (1980 and 1977) examined flows around spheres and hemisphere-cylinders in a wind tunnel. These studies showed that there is a separation from a fully submerged body that forms a continuous vortex arch where either end of the vortex is rooted at the wall. Flow of this nature cannot be approximated as two dimensional but must be considered as fully three dimensional. Okamoto concluded that the arch vortices are shed, travel a short distance downstream of the obstacle and then the ends of the arch vortex become fixed to the bed at one location. The upper parts of the arch vortex cannot be held fixed and continue to move downstream producing a rotation of the arch vortex about the fixed point on the bed. Okamoto found that a strong downwash behind the obstacle prevents the upper parts of the arch vortex from being advected completely away from the obstacle. He stated that the downwash ultimately rotates the arch vortex so that it is parallel with the bed at which time it is destroyed.

2.2.4 Single Hemisphere in Open Channel Flow

Shamloo (1997) identified four distinct regimes of flow around a hemisphere placed in an open channel on a smooth bed. When the depth of flow (d) was more than four times the height of the obstacle (h), the fluid at the free surface did not mix at all with the fluid in the wake of the obstacle and the free surface was not noticeably affected by the presence of the obstacle. Flow satisfying this condition ($d/h \geq 4$) was classified as Regime 1. In an

intermediate region of relative flow depths ($1.3 \leq d/h < 4$), the fluid at the free surface also did not mix with the wake fluid from the obstacle however the free surface was affected by the presence of the obstacle. This flow condition was classified as Regime 2. Regime 3 exists in a narrow band of relative depths ($1.1 \leq d/h < 1.3$) and is characterized by strong mixing of fluid from the surface to the bed downstream of the obstacle. Regime 4 occurred when $d/h < 1.1$ and could generally be approximated by a two dimensional flow with strong recirculating flow behind the obstacle. Under these flow conditions a classical Karman vortex street was observed to form in the obstacle wake.

Fisher and Klingeman (1984) studied the scour behavior of a mobile material around a fish habitat obstacle. A large scour hole formed in front of the obstacle and had a similar general form to that found by Ahmed (1994) for cylindrical bridge piers. The obstacles used in the Fisher and Klingeman study were rigidly fixed and thus no interaction between the obstacle position and the scour hole was investigated.

2.3 Considerations Associated with a Mobile Bed

2.3.1 Single Hemisphere in Open Channel Flow

When the fluid encounters an obstacle to flow such as a hemisphere placed on a flat, mobile bed the fluid is accelerated around the obstacle. This fluid acceleration produces the highest initial bed shear stresses at the sides of the obstacle which in turn experience the first signs of scouring. In front of the obstacle it is the presence of the HS vortex that produces high bed shear stresses. The HS vortex ultimately produces the deepest scour in front of the obstacle once steady state is reached (Fisher and Klingeman,1984). Shamloo (1997) found that the shape of the scour hole is strongly dependent on the shape of the obstacle.

2.3.2 Obstacle Groups

One study focused on the interaction of pile groups and the group influence on local scouring (Hannah, 1978). Hannah found that pile groups placed in close proximity compress HS vortices between them thus amplifying the angular velocity of the vortex. He credited this increase in angular velocity with the tendency for pile groups to scour deeper than lone piles. Once the center separation of the piles was reduced to 2 pile diameters or less and the angle of attack (angle from streamwise to the center to center line between two piles) was high, Hannah found that the compressed HS vortex effect dominates the scour process producing deep, steady-state scour. Hannah further observed that vortices (Karman vortices) shed from the side of a pile that encounter piles downstream will tend to increase the scouring of those downstream piles. He attributed this to the fact that the shed vortices are attached to the bed and "provide pockets of low pressure which assist in lifting material from the scour hole". As an extreme, Hannah found that the piles in a group display independent behavior when the center separation of the piles is six times the pile diameter or greater.

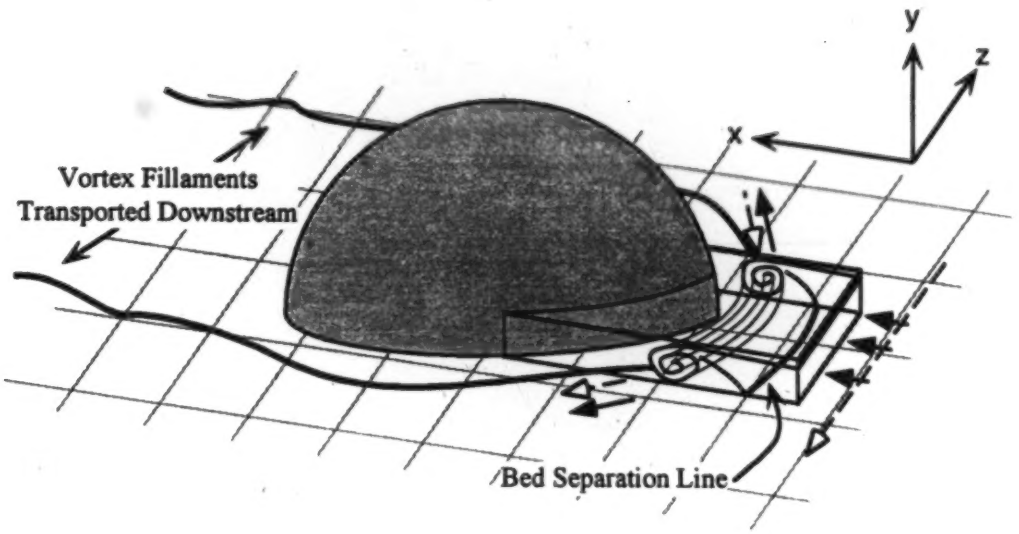

Figure 2.1 Fluid movement and vorticity orientation for the horseshoe vortex

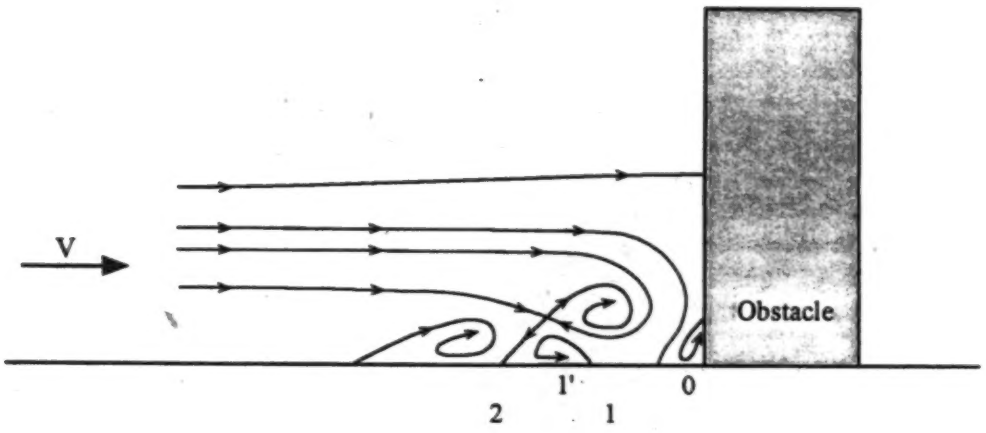

Figure 2.2 Wind tunnel vortex cascade (Adapted from Baker - 1980)

CHAPTER 3

EXPERIMENTAL SETUP AND TESTING PROGRAM

3.1 Laboratory Facilities

The experiments for this research were conducted in a flume (Figure 3.1) consisting of two sections, a straight section of length 13.4 m followed by a curved section of length 17.2 m. Water was pumped from a dedicated sump to a head tank that emptied directly onto the straight portion of the flume. The obstacles were placed 7.6 m from the head tank and 6.8 m upstream of the entrance to the 270° curved section. At the end of the curved section a tailgate controlled the depth of flow to within ± 1 mm throughout the flume. The width of the flume was 1.07 m and the maximum depth of flow was 18 cm. The flow rate in the flume could be measured with a magnetic flow meter to within ± 0.01 L/s with a maximum possible flow rate of 40 L/s.

3.2 Model Criterion

3.2.1 Prototype River Characteristics

Many rivers in southwest Alberta contain artificial fish habitat structures. A listing of rivers that have had fish habitat structures added can be found in the report by R. L. & L. Environment Services Ltd. (1994). The range of river sizes listed in this report was great with the largest rivers being the Crowsnest, Castle, Waterton and Oldman rivers. The number of fish habitat sites contained in each of these rivers are 10, 1, 3 and 2 respectively. These four rivers were selected as the prototype rivers to model since the characteristics of larger rivers are not as difficult to approximate in the laboratory. All river properties such as annual flow rates and typical channel geometry were obtained from Kellerhals, Neill and Bray (1972).

3.2.2 Model Froude Number

The natural rivers being modeled experience enormous changes in discharge throughout the seasons. As was stated in Chapter 1, the hydraulics of a rock cluster is important at both high and low discharges. During high discharge the obstacles will be deeply submerged and would most appropriately be modeled using a Reynolds criterion. Conversely during low discharge the obstacles may break the water surface or will be shallowly submerged and should be modeled using Froudian considerations. In this study it is assumed that the hydraulic performance of the fish habitat structures will be most significant for fish during periods with relatively low flows. These low flow periods will have depths of flow of approximately 1 m. Since the fish habitat structures are likely to have elements that are approximately 1 m in diameter or height we can assume that these elements will not be deeply submerged and can be modeled as a Froudian flow.

In choosing model hydraulic parameters the long-term mean annual flow was used. This value is much smaller than the 2-year flood and should reasonably reflect the low flow conditions during spawning and migration. A model Froude number was computed to be approximately 0.25 with a relevant range of $0.2 < Fr < 0.25$. The Froude number was computed as:

$$Fr = \frac{V}{\sqrt{gd}} \tag{3.1}$$

where V is the free stream velocity in m/s, g is the acceleration due to gravity in m/s^2 and d is the depth of flow in meters.

3.2.3 Obstacle Geometry and Placement

Two types of obstacles were used in this research; natural rocks and styrofoam hemispheres. The rocks that were used in the flume were cut from larger rocks with a diamond saw. The larger rocks from which the obstacles were cut were rounded and were of the same approximate size as the styrofoam hemispheres. Two different diameters (D = 5 cm and D = 10 cm) of styrofoam hemisphere were selected for testing. To avoid damaging the delicate styrofoam surface no mechanical cutting tools were used and each sphere was approximately cut in half by hand. Three hemispheres were obtained from 10 cm diameter spheres such that the height (h) of each hemisphere, when placed flatly on the flume bed, was in the range $4.5 \leq h \leq 4.7$ cm. Similarly, three hemispheres were cut from 5 cm diameter styrofoam spheres and had heights in the range $2.2 \leq h \leq 2.4$ cm. The rock obstacles were slightly less uniform with a base diameter ranging from $8.0 \leq D \leq 9.0$ cm and a range of obstacle heights of $7.9 \leq h \leq 8.5$ cm. Representative values of D and h for the rock obstacles were taken to be 8.5 cm and 8.2 cm respectively.

Accurate placement of all styrofoam obstacles was ensured by placing the edges of the obstacles relative to a grid drawn on the painted bed surface. It is believed that the styrofoam obstacles could be placed in this manner with an accuracy of $\pm$ 1 mm. To counter the buoyant force the styrofoam spheres were glued to the bed during the tests.

The irregular shapes of the rock obstacles did not permit their placement in the same manner as the styrofoam obstacles. To maintain a consistent presentation to the flow, each of the rock obstacles were placed with a consistent orientation by marking the upstream side. The approximate center of the obstacle was then found and marked at the top of the rock. The desired center for each obstacle was computed and then marked on the bed. A point gauge was used to transfer the bed coordinate vertically and the center mark on top of the obstacle was positioned beneath the point gauge. It was believed that

positioning the obstacles in this manner could be done to an accuracy of ± 2 mm. Once placed, the rock obstacles remained stationary under all flow conditions due to their submerged weight.

A typical configuration of obstacles is illustrated in Figure 3.2 with the upstream obstacle referred to as the Leading Element (LE) and the remaining two obstacles referred to as the Trailing Elements (TEs). Three geometrical properties were intentionally varied in these tests: the obstacle diameter (D), the center to center spacing of the two TEs (S'D) and the center to center spacing of the LE to either of the TEs (SD). The parameters S and S' are scalars of the obstacle diameter and are therefore dimensionless. Throughout the experiments it was endeavoured to maintain the values of S and S' as approximately equal. This equality is deemed appropriate since the ultimate application of this research will be design recommendations for field structures where a complicated relationship between S and S' would not be practical. The testing program permitted S and S' to have different values however the ratio of S/S' was maintained at 0.94 ± 0.06. Throughout this thesis the spacing of the obstacles will be expressed numerically as S/S'. The grid that was marked on the bed surface had dimensions of 10 cm in the streamwise direction and 5 cm in the transverse direction.

3.3 Data Collection

3.3.1 Flow Visualization

All data contained in this thesis were obtained through visualization of the flow. Dye tracing was used as the primary visualization technique. Application of dye was through a long hypodermic needle connected to a reservoir. Red food coloring with a specific gravity slightly greater than unity was used at full concentration or diluted if the flow structures being visualized were sensitive to tracer density.

3.3.2 Capturing an Image from a Videotape.

All images used in the analysis were captured using NIH Image 1.52. NIH Image is a public domain Macintosh program designed for digital image processing and analysis. A Macintosh Quadra 700 computer running NIH Image was connected to a VHS format video player through a Data Translation Framegrabber card. This arrangement allows the user to capture images from the video player at rates ranging between 5 and 20 frames per second depending on the size of image captured. All images were captured with an 8 bit greyscale colour pallet. Once an image had been captured, the brightness and contrast of the image were manually adjusted for maximum clarity using the public domain Macintosh program GraphicConverter 2.5.1.

3.3.3 Data Extracted from Images

Quantitative data were obtained from the captured images by utilizing the measurement capabilities of NIH Image. To accommodate the possibility that each of the captured images may be obtained at different levels of zoom a scaling factor was calibrated to the grid painted on the flume bed. Calibration may be done at any point in the image thus allowing for rough scaling of oblique images. Once the calibration is completed, measurements were taken directly from the image. It was believed that the data extracted from the images in this way was accurate to $\pm$ 3 mm.

3.4 Testing Program

Extensive testing was carried out on the styrofoam spheres. For both the 10 and the 5 cm diameter hemispheres, a total of 24 experiments were carried out consisting of 6 different obstacle spacings and 4 depths of submergence. The relative depth of flow (d/h) was varied from a maximum of 3 to a minimum of 0.5 where d is the depth of flow and h is the height of the obstacle. Six obstacle spacings were used such that the parameters S and S' varied between a maximum of S = 1.8, S' = 2.0 and a minimum of S = S' = 1.0. A reduced

testing program of 9 experiments was used for the rocks placed on the rigid bed. In these experiments three depths of submergence were used such that the relative depth was at maximum d/h = 1.5 and at minimum d/h = 0.5. Three obstacle spacings were used such that the parameters S and S' varied between a maximum of S = 1.8, S' = 2.0 and a minimum of S = 1.1, S' = 1.2. An additional test was conducted for the 5 cm diameter hemispheres where the flow depth was slightly greater than half the obstacle height. This change in flow conditions was necessary to better visualize a cascade of HS vortices in front of the cluster. A complete listing of the testing program is presented in Table 3.1.

Each of the tests described above was conducted on a rigid and smooth (RS) bed. In addition to this testing program, a single test was conducted using the rock obstacles on a mobile and rough (MR) bed of loose sand. The grain size distribution of the sand is presented in Shamloo (1997) as the sand with D50 = 0.25 mm. Water was permitted to flow for 5 days with a relative depth of d/h = 1.5. The bed had not yet reached a steady state when the test was terminated. However, little change was observed over the last 24 hours of the test. The initial spacing condition for the obstacle was S/S' = 1.0/1.0 and each obstacle was seated approximately 5 mm below the surface of the sand.

	RS											MR
	D = 10 cm				D = 5 cm				D = 8.2 cm			D = 8.2 cm
Spacing	d=h/2	d=h	d=2h	d=3h	d=h/2	d=h	d=2h	d=3h	d=h/2	d=h	d=1.5h	d=1.5h
1.8/2.0	x	x*	x	x	x	x	x	x	x	x	x	
1.7/1.8	x	x		x	x	x	x	x				
1.4/1.6	x	x	x	x	x	x	x	x	x	x	x	
1.3/1.4	x	x	x	x	x	x	x	x				
1.1/1.2	x	x	x	x	x	x	x	x	x	x	x	
1.0/1.0	x	x	x	x	x	x	x	x				x
V	10.5	14.8	21.0	25.8	7.7	10.9	15.6	19.2	14.1	19.9	24.7	24.7
R	1758	4973	14305	26428	708	2003	5844	10846	4310	12191	23242	23242

Multiple Vortices (D = 5 cm)

d = 1.4 cm

V = 8.3 cm/s

R = 1160

- x* Indicates that only a Bed Shear Profile (BSP) image was captured
- Reynolds number is computed using the depth of flow (d) as the characteristic length
- The water temperature for the tests ranged from 5 C to 15 C so viscosity of the water was taken to be that at 10 C.

v = 1.31E-06 m^2/s

Table 3.1 Experimental testing program

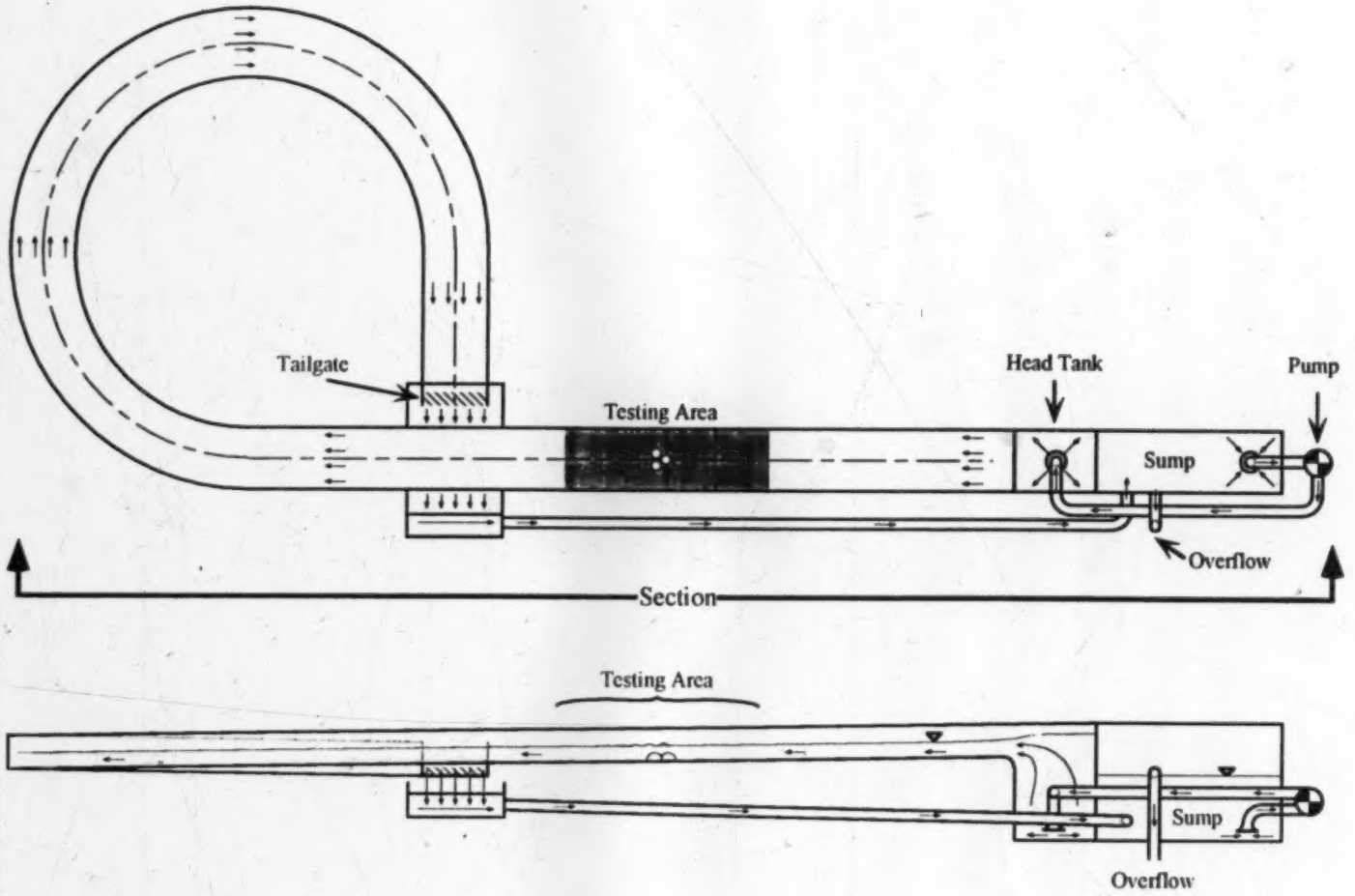

Figure 3 1 Experimental setup

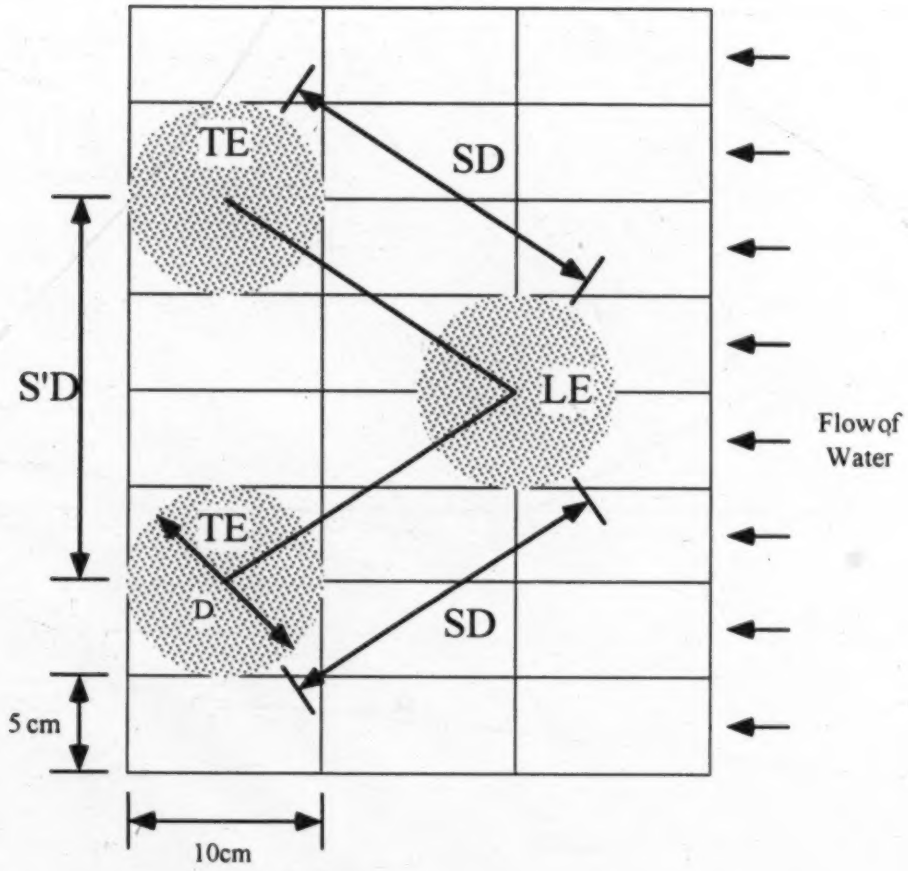

Figure 3.2 Plan view of obstacle geometry

CHAPTER 4

EXPERIMENTAL RESULTS

4.1 Local Flow Effects of the Cluster on a Rigid Bed

4.1.1 Separation Profile

Figure 4.1 is a schematic of what will be hereafter referred to as a Separation Profile or SP. The dark lines around each of the obstacles represents the flow separation line from the bed. This feature is visualized by injecting dye into the laminar sublayer around the obstacles at the bed separation line. Between the separation line and the obstacle the bed shear vector was oriented away from the obstacle whereas outside the line the bed shear vector was oriented towards the obstacle. Five length scales (a, b, c, e and f) were chosen to represent the position of the separation lines relative to the obstacles. With the exception of the length scale a, each of the recorded values for these length scales were computed as the average between the left and the right measured values. Each of the length scales were non-dimensionalized with the obstacle diameter and the normalized scales were plotted against either the relative depth (d/h) or the spacing parameter (S). These plots are presented in Figures 4.2 to 4.19. Figures 4.2 to 4.11 do not include the experimental data where D = 5 cm and d = h/2. Figures 4.12 to 4.19 include this data since the maximum values on the ordinate are significantly larger to accommodate this data. The figures containing c/D did not need to be replotted.

Appendix A contains all of the SP images captured from videotape. It was from these images that the length scales a, b, c, e and f were taken. For each figure in Appendix A spacing increases as one moves toward the top of the page and depth increases as one moves to the right of the page. Figures A1 to A3 contain the SP images associated with the styrofoam hemispheres of diameter D = 5 cm. Figure A1 contains all the SP images associated with the smaller three obstacle spacings. Figure A2 contains all the SP images

associated with the larger three obstacle spacings. Figure A3 combines all the SP images from A1 and A2 excluding the images where D = 5 cm and d/h = 0.5. Figure A4 contains all SP images with the styrofoam hemispheres of diameter D = 10 cm. Figure A5 contains all SP images with the natural rocks of diameter D = 8.2 cm.

Note that at the end of each experiment the styrofoam hemispheres had to be removed from the bed. Since the obstacles were glued to the bed their removal occasionally peeled paint off the bed surface that appears as dark areas in the images from Appendices A and B. These dark areas could be mistaken for dye however a comparison of images from two different experiments will reveal irregularly shaped dark areas with identical outlines and may be ignored.

4.1.2 Horseshoe Vortex Systems

4.1.2.1 LE Horseshoe Vortex Cascade, D = 5 cm and d/h = 0.5

When D = 5 cm and d/h = 0.5 a cascade of HS vortices were observed to form in front of the LE. When this cascade was present then it formed around the entire cluster regardless of the spacing of the obstacles. The bed separation line was observed to be located upstream of the LE a distance of (length scale a in Figure 4.1) several times the diameter of vortex 1. The general structure of these vortices are shown in Figure 4.20a. When viewed with a left to right flow, four primary vortices were observed to rotate clockwise (1, 2, 3 and 4) while four secondary vortices were observed to rotate counter clockwise (0, 1', 2' and 3'). All of these vortices could be observed when the Reynolds number based on depth was R = 1160 while vortices 0, 1, 1', 2, 2' and 3 were visible when the Reynolds number was R = 708. Vortices 1, 1' and 2 are visible in Figure 4.20b while the four primary vortices (1, 2, 3 and 4) are visible in Figure 4.20c. A plan view of the vortex cascade is presented in Figure 4.21 with a supporting schematic. The top half and the bottom half of Figure 4.21a were taken at different times and later combined to create a

single image. Combination of the two images to form a single image was necessary since visualization of the primary or minor vortices required that dye be injected at different levels in the flow. Visualizing the primary vortices in Figure 4.20a required that dye be injected below the β streamline. To visualize the minor vortices, dye was injected between the two streamlines α and β. The α streamline terminates at the bed immediately upstream of vortex 0 while the β streamline terminates on the bed directly beneath vortex 4. It was observed that injecting dye immediately upstream of the termination point for the α streamline permitted dye to be transported up to and be entrained by vortices 1', 2' and 3'.

A HS vortex was also observed to form immediately beneath the surface and in front of the LE. An image of the vortex filament wrapping around the LE is contained in Figure 4.20d. The dye needle is visible as the dark vertical line and it displays a horizontal discontinuity at the point where it crosses the surface of the water. From the tip of the needle can be seen a very small circular feature that is the vortex entraining the dye. A reflection of the dye contained in the surface HS vortex filament can be seen in Figure 4.20d and may be ignored

4.1.2.2 LE Horseshoe Vortex, Other than D = 5 cm and d/h = 0.5

Under most flow conditions in this study a single HS vortex was observed to form in front of the LE. This vortex corresponds to vortex 1 in Figure 4.20a. The bed separation line was observed to be located upstream of the LE a distance (length scale a in Figure 4.1) slightly greater than the diameter of the HS vortex. Under these conditions it was possible, although difficult, to see vortices 0 and 1'. It was not possible to see a surface HS vortex.

When the relative flow depth and the obstacle spacing were large ($d/h \geq 1.5$, $S/S' \geq 1.7/1.8$) the HS vortex filaments from the LE were deflected to flow between the TEs (Figure 4.22). As obstacle spacing became smaller ($1.3/1.4 < S/S' \leq 1.4/1.6$), the filaments were lifted from the bed by the TE HS vortices to flow at some mid elevation. At even smaller spacings ($1.0/1.0 < S/S' \leq 1.3/1.4$) the strong vortex systems behind the LE did not permit visualization of the filaments. It was only when the obstacles were touching each other ($S/S' = 1.0/1.0$) that the HS vortex filaments from the LE were observed to move around the outside of the TEs.

When the relative depth was small and the obstacle spacing was large ($d/h \leq 1.0$, $S/S' \geq 1.7/1.8$), the LE HS vortex filaments passed between the two TEs just as they did for large relative depths. When the obstacle spacing was reduced to ($1.1/1.2 \leq S/S' \leq 1.4/1.6$) then the LE HS vortex filaments were broken up by the presence of the TE HS vortices. As when the relative depth was large, when the obstacles were touching each other the LE HS vortex filaments were deflected entirely around the cluster.

4.1.2.3 TE Horseshoe Vortex

Excluding tests where $D = 5$ cm and $d/h = 0.5$, when the obstacle spacing was $S/S' \geq 1.4/1.6$ HS vortices similar to vortex 1 in Figure 4.20a were observed to form in front of the TEs. Vortex filaments from these HS vortices were observed to be carried behind the TEs in a similar fashion as shown for the LE in Figure 4.22. Between the TEs the reduced flow area sped up the rotation of the vortices. Visualization of the TE HS vortex filaments between the TEs was difficult when $1.3/1.4 \leq S/S' \leq 1.4/1.6$. When $S/S' = 1.1/1.2$ it was not possible to visualize the TE HS vortex filaments between the TEs and the TE HS vortex filaments on the outside of the TEs were also more difficult to visualize. As indicated in Section 4.1.2.2, when $S/S' = 1.0/1.0$ the LE HS vortex filaments

were observed to flow around the cluster so that separate HS vortices were not able to form in front of the TEs.

4.1.3 Arch Vortex

When the obstacles were spaced at S/S' ≥ 1.7/1.8 and d/h ≥ 1.5, the arch vortices shed freely from the LE (Figure 4.23). The tops of these shed arch vortices were observed to gradually extended vertically into the main flow. The sides of the arch vortex also shed from the LE, however once freely moving they were destabilized by the presence of the TEs. When S/S' ≤ 1.4/1.6 and d/h ≥ 1.5, the vortices shed from the top of the LE were observed to extend upwards into the main flow at an accelerated rate (Figure 4.24) compared to that for large obstacle spacings. The white arrows in Figure 4.24 point to the tops of successive vortices shed from the top of the LE. Under these conditions the sides of the arch vortex were held in place by the TEs with fluid motion described by the black arrows in Figure 4.25a. The orientation of the vortices are shown by the dotted arrows in Figure 4.25b. Movement of the fluid around the LE created a strong, stable vortex on either side of the LE the core of which is denoted by the grey arrows. The vortices from either side of the LE changed orientation from perpendicular to the bed behind the LE to parallel to the bed between and above the TEs. The combined influence of these vortices produced a strong vertical flow between them. When S/S' ≤ 1.4/1.6 and d/h = 1.0 no vortices may be shed from the top of the LE however the presence of these two vortices created a very strong surface boil between the two TEs (Figure 4.26). At obstacle spacings of (S/S' ≤ 1.4/1.6) it was not possible to visualize the shedding of arch vortices from the top or between the TEs. At large obstacle spacings (S/S' ≥ 1.7/1.8) the shedding of arch vortices was similar to that of the LE.

4.1.4 Flow Separation Behind Obstacles

For large obstacle spacings ($S/S' \geq 1.7/1.8$) and $d/h \geq 1.0$, fluid flowing around both the LE and the TEs was observed to separate from the obstacle surface such that the separation line approximately bisected the obstacle. This observation varied little for the TEs under all flow conditions. For moderate obstacle spacings ($1.3/1.4 \leq S/S' \leq 1.4/1.6$) separation from the LE did not occur near the bottom. At small obstacle spacings ($S/S' \leq 1.1/1.2$) only a small area on the rear top of the LE remained as the separated region. This small separated area is shown in Figure 4.27 both in plan (a) and from the side (b). The bottom of the separated region did not extend below the top half of the obstacle and the fluid that separates at the lowest point was observed to be moving vertically.

4.2 Extended Flow Effects of the Cluster on a Rigid Bed

4.2.1 Bed Shear Profile

Appendix B contains a series of images that are called the Bed Shear Profiles or BSPs. Each page contains four images where the depth of flow is varied and both the obstacle spacing and the obstacle diameter were held constant. The depth of flow is smallest in the bottom left image while the depth of flow is greatest in the top right image. The patterns in these images were created by allowing the flowing water to smear lines of dye injected into the laminar sublayer of the bed. The direction of dye smearing indicates the orientation of the bed shear vector. When the cluster was fully submerged ($d/h \geq 1.5$) the direction of the bed shear vector was not observed to be affected at distances exceeding 1 obstacle diameter from the cluster. When the cluster was not fully submerged ($d/h \leq 1.0$) then the bed shear vector was observed to be significantly affected at distances from the cluster exceeding 3 obstacle diameters. When $D = 5$ cm and $d/h = 0.5$ the cluster was observed to produce an extreme change in direction of the bed shear vector at distances exceeding 5 obstacle diameters. Changes to obstacle spacing were not observed to

significantly affect the direction of the bed shear vector at distances exceeding 1 obstacle diameter from the cluster.

4.2.2 Wake of the Obstacle Clusters

When the relative depth was small (d/h = 0.5) there was observed a classical train of Karman vortices in the wake of the obstacle (Figure 4.28). This observation was made regardless of the obstacle spacing. When the relative depth was d/h = 1.0 then a symmetrical set of vortices were observed to form in the wake of the obstacle cluster (Figure 4.29). These vortices were created when fluid alternately surges between the TEs and around them. Figure 4.29 was taken just after the fluid surged between the TEs. This phenomenon was only observed when the obstacle spacing was large. When the relative depth was large (d/h $\geq$ 1.5) and the obstacle spacing was relatively small (S/S' $\leq$ 1.3/1.4), the wake fluid from adjacent obstacles mixed readily. This mixing produced regions of backflow behind the TEs that were larger than could be maintained by a single obstacle. These regions of backflow were observed to be linked behind the TEs when obstacle spacing was small (S/S' $\leq$ 1.1/1.2). When the obstacle spacing was increased such that S/S' $\geq$ 1.4/1.6 the wake fluid from adjacent obstacles did not readily mix (Figure 4.30).

4.3 Effects of a Cluster on a Mobile Bed

Results for the single test where the obstacles were placed on a mobile bed material are presented in Figure 4.31. The dotted and solid circles in Figure 4.31b represent the initial and final positions of the obstacles respectively. The dots and arrows within each of the circles respectively represent the center and orientation of the obstacles as marked at the start of the experiment. These dots and arrows were marked on the obstacles with a pen and therefore represent the absolute translation and rotation of a particular point at the top of each obstacle when viewed from above. A single HS vortex formed around the cluster that produced a significant scouring. All of the obstacles were observed to lean

into the HS vortex scour hole. Leaning into the scour hole produced an upstream translation for the LE. Leaning into the scour hole produced an upstream translation and an outward movement for the TEs. Each obstacle translated upstream approximately the same distance and the height of each obstacle was reduced by approximately one third. The TEs were observed to rotate such that the original upstream face of the obstacle turned inward to face the LE. No rotation of the LE was observed.

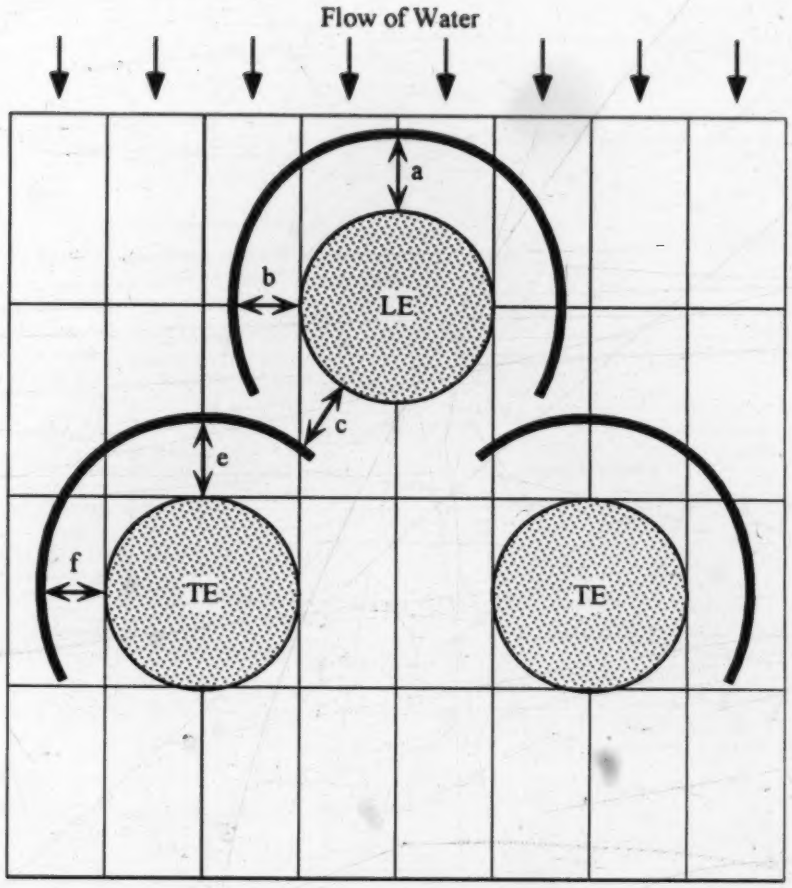

Figure 4.1 Separation profile length scales

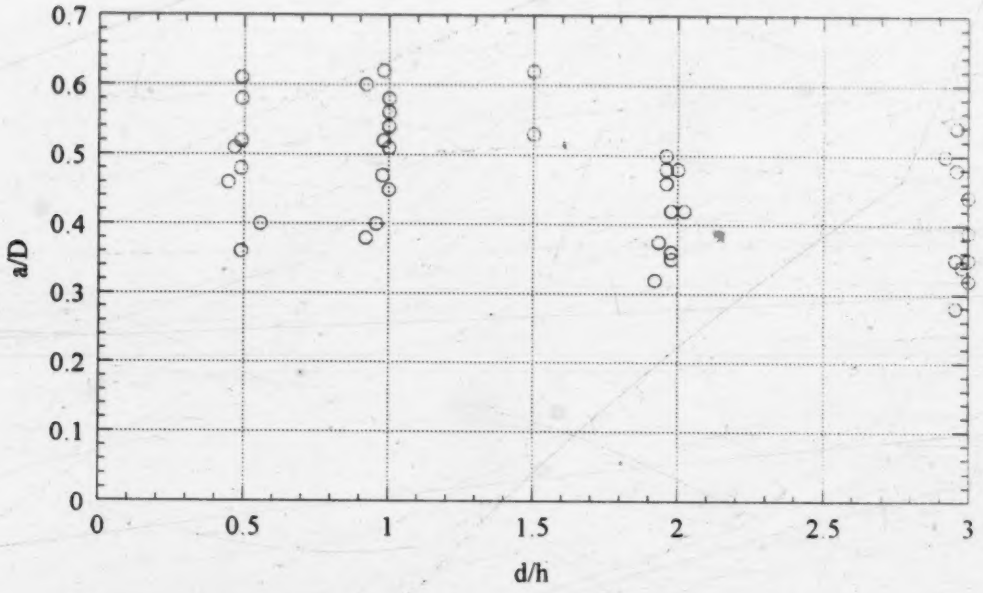

Figure 4.2 Normalized length scale "a/D" as a function of d/h

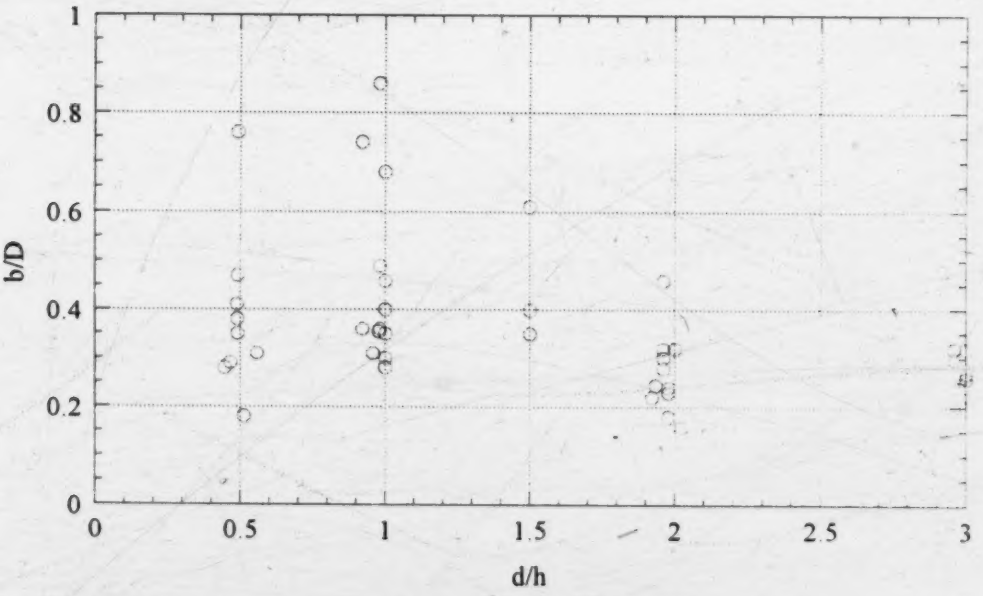

Figure 4.3 Normalized length scale "b/D" as a function of d/h

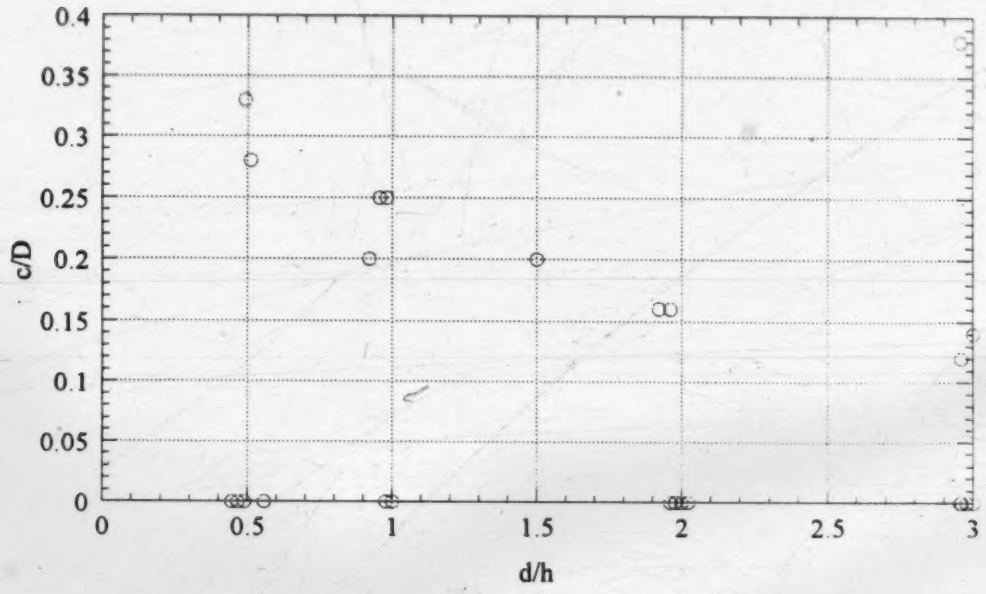

Figure 4.4 Normalized length scale "c/D" as a function of d/h

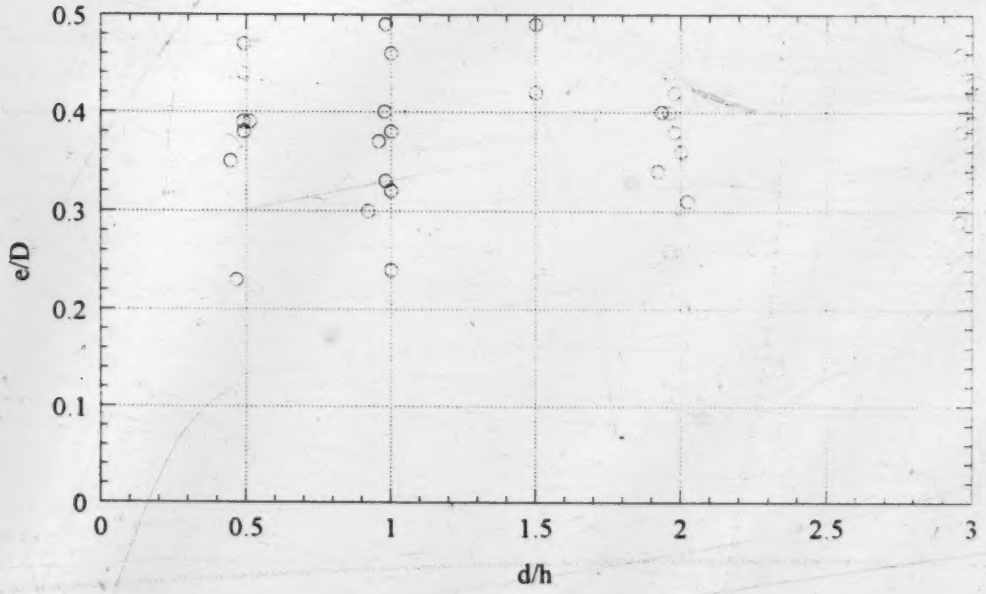

Figure 4.5 Normalized length scale "e/D" as a function of d/h

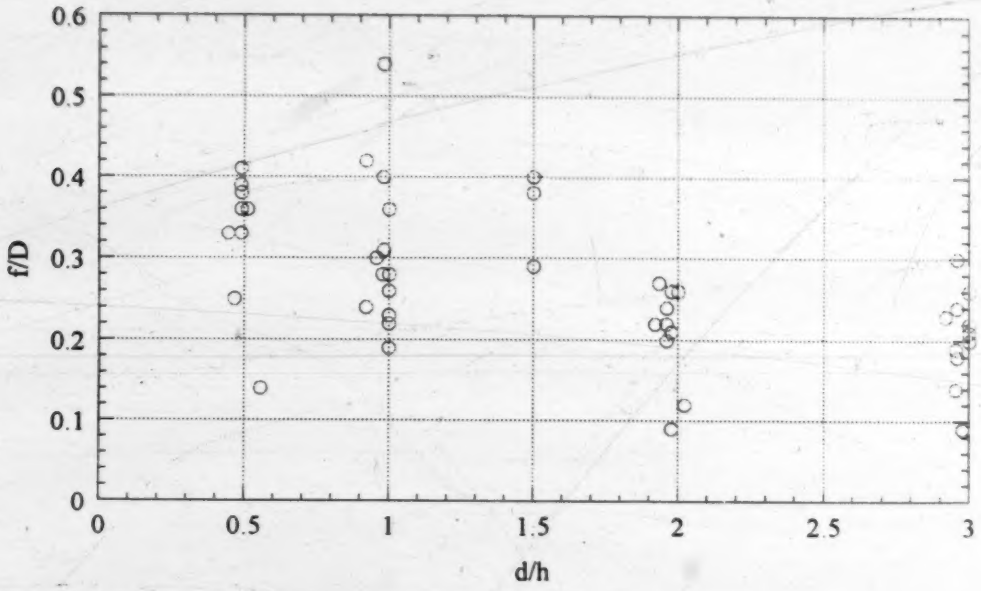

Figure 4.6 Normalized length scale "f/D" as a function of d/h

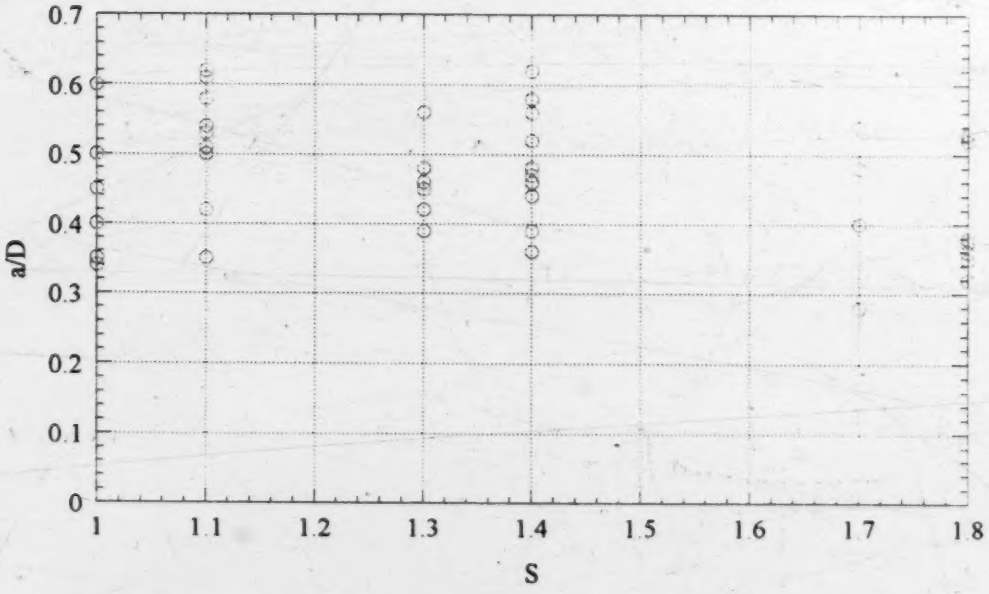

Figure 4.7 Normalized length scale "a/D" as a function of the spacing parameter S

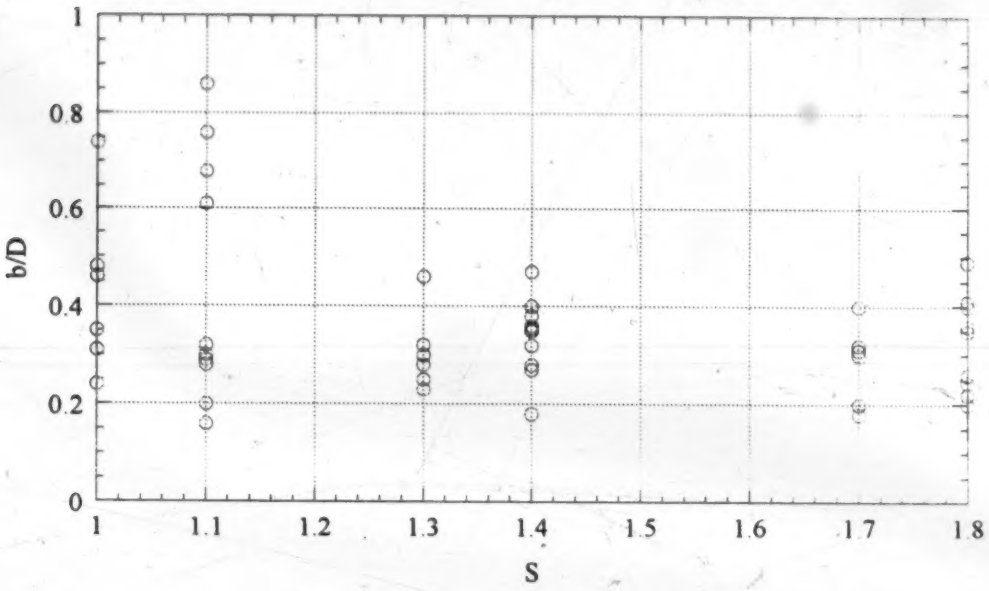

Figure 4.8 Normalized length scale "b/D" as a function of the spacing parameter S

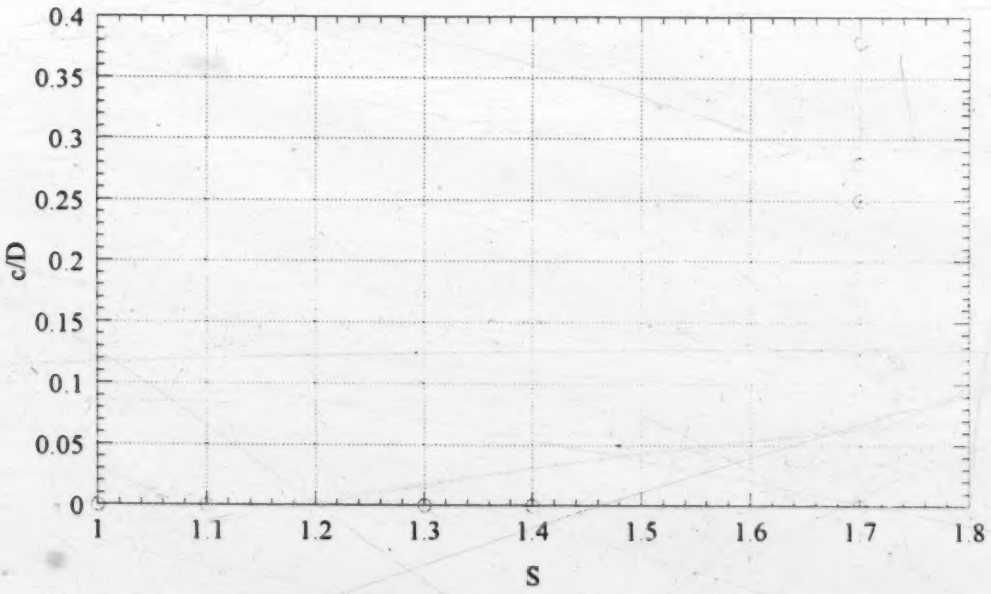

Figure 4.9 Normalized length scale "c/D" as a function of the spacing parameter S

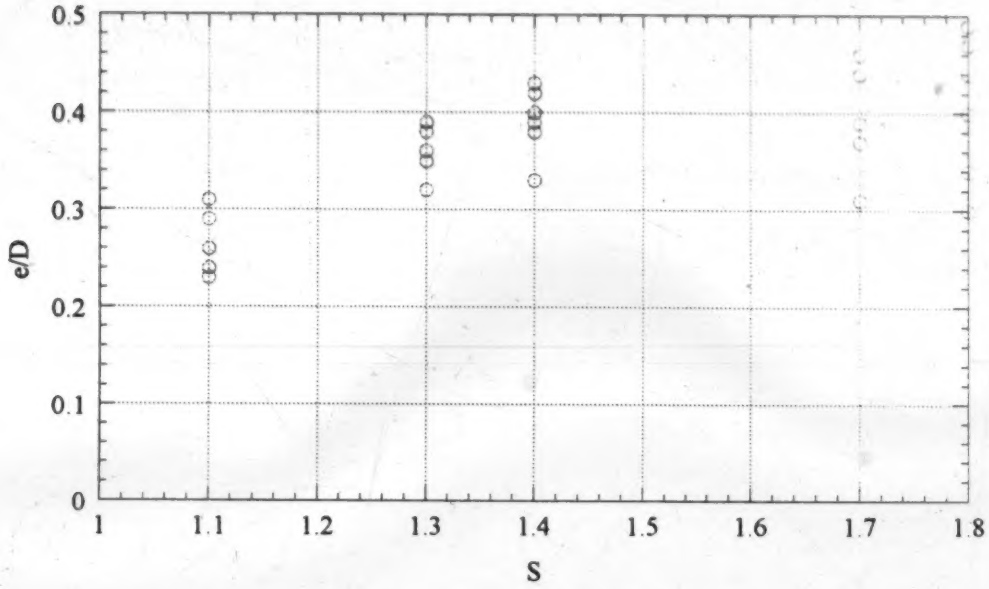

Figure 4.10 Normalized length scale "e/D" as a function of the spacing parameter S

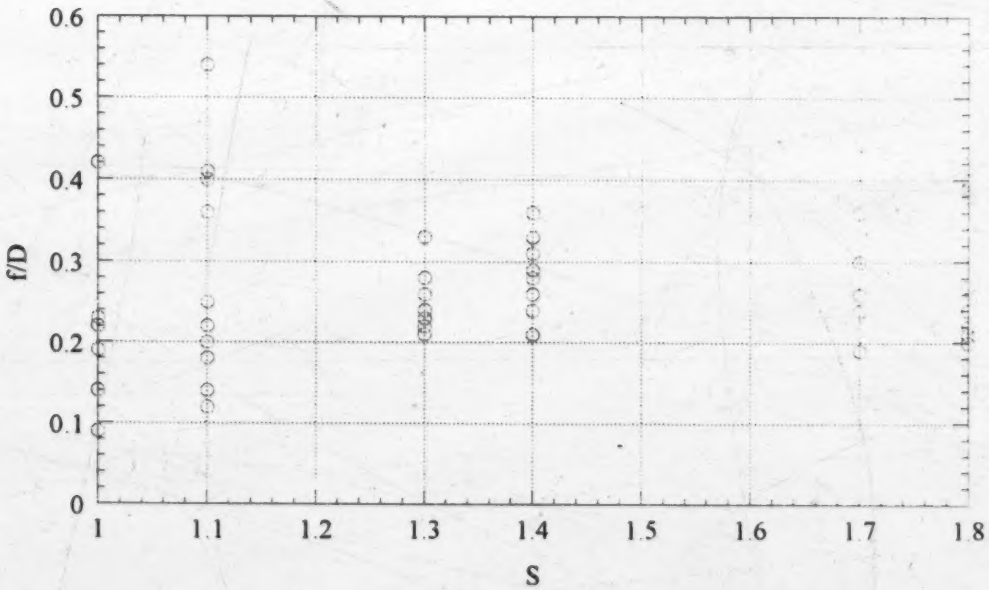

Figure 4.11 Normalized length scale "f/D" as a function of the spacing parameter S

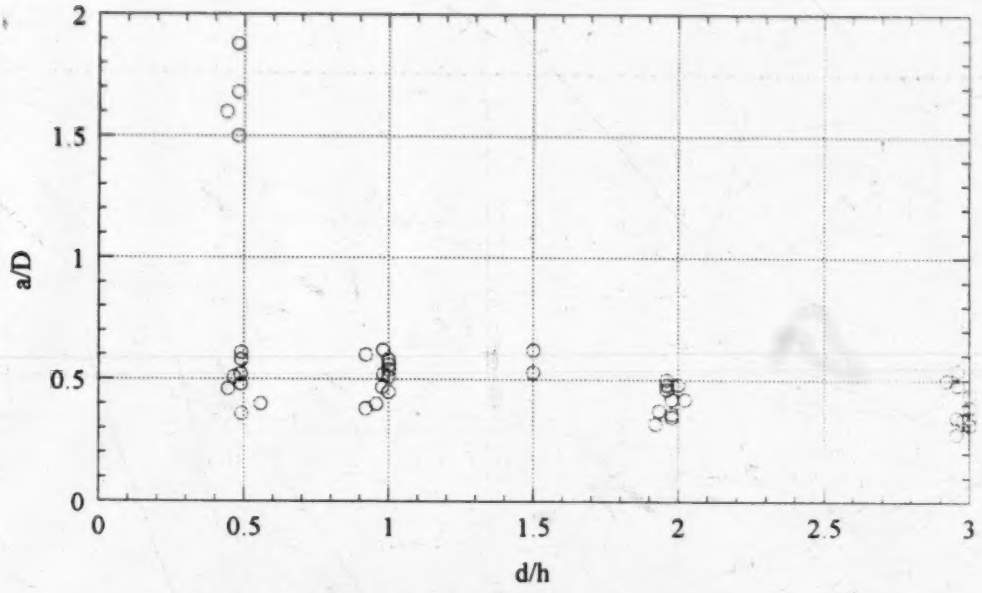

Figure 4.12 Normalized length scale "a/D" as a function of d/h
(Including RS5-S/S', d=1.2 cm)

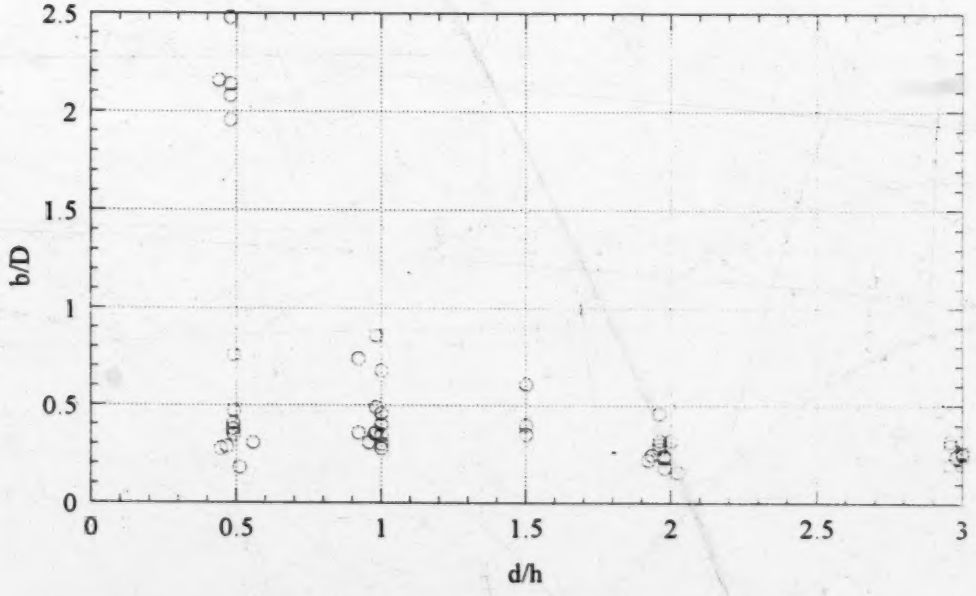

Figure 4.13 Normalized length scale "b/D" as a function of d/h
(Including RS5-S/S', d=1.2 cm)

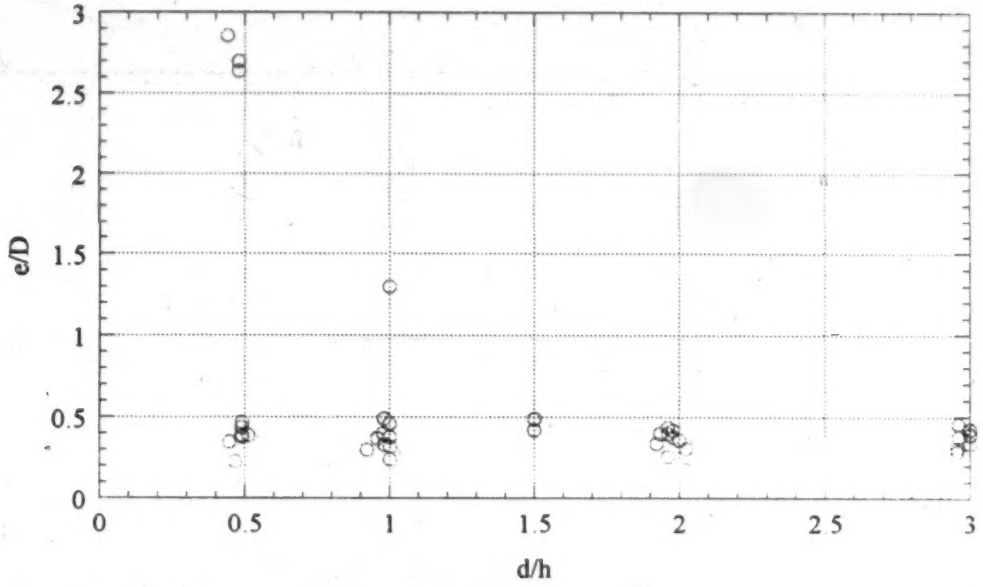

Figure 4.14 Normalized length scale "e/D" as a function of d/h
(Including RS5-S/S', d=1.2 cm)

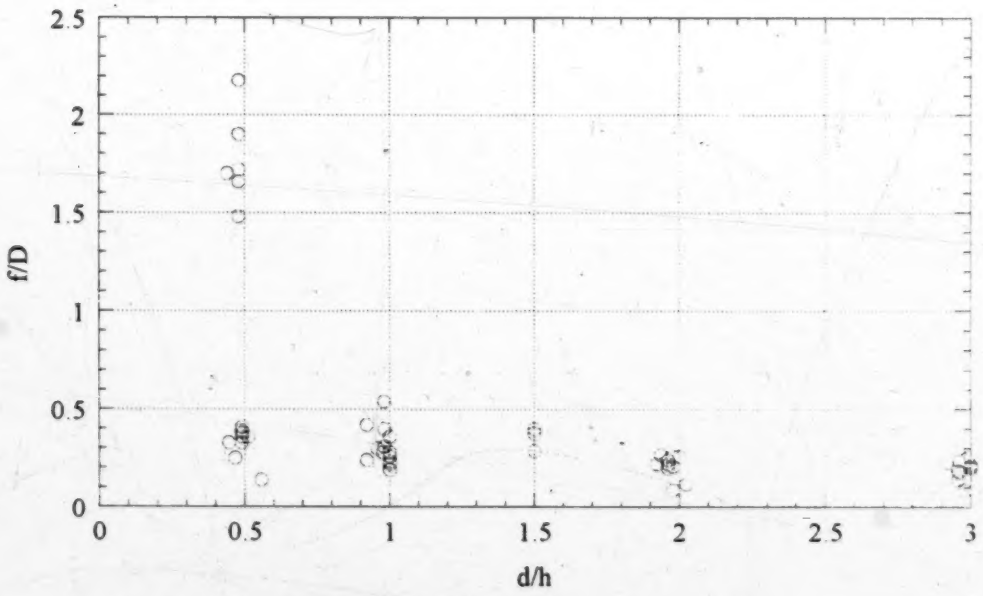

Figure 4.15 Normalized length scale "f/D" as a function of d/h
(Including RS5-S/S', d=1.2 cm)

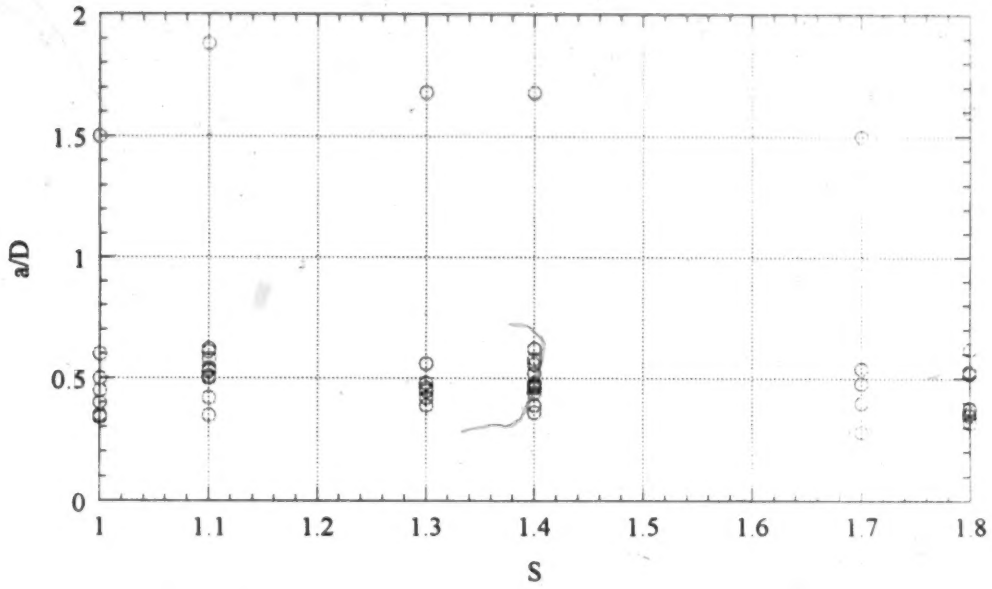

Figure 4.16 Normalized length scale "a/D" as a function of the spacing parameter S (Including RS5-S/S', d=1.2 cm)

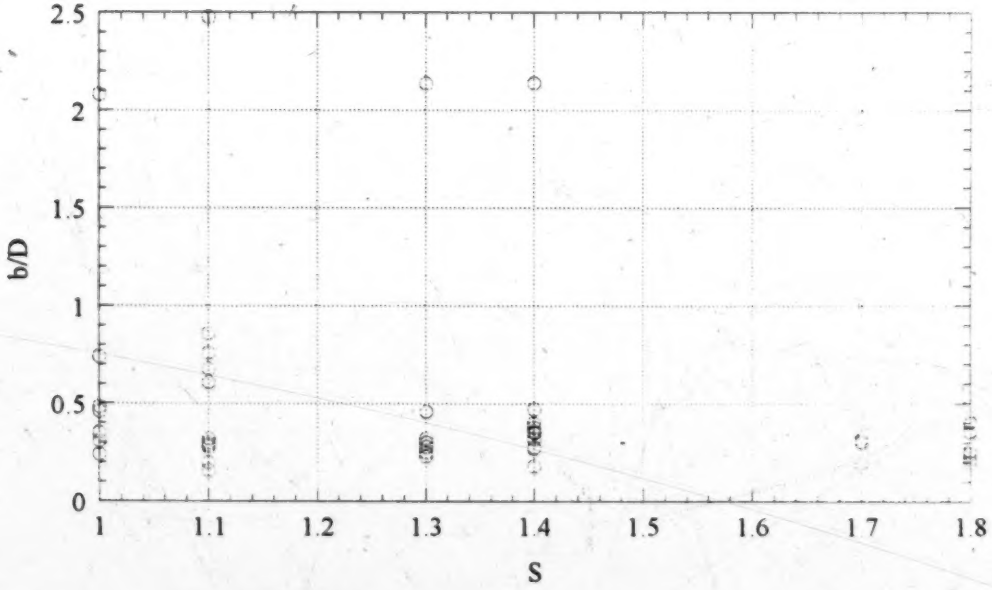

Figure 4.17 Normalized length scale "b/D" as a function of the spacing parameter S (Including RS5-S/S', d=1.2 cm)

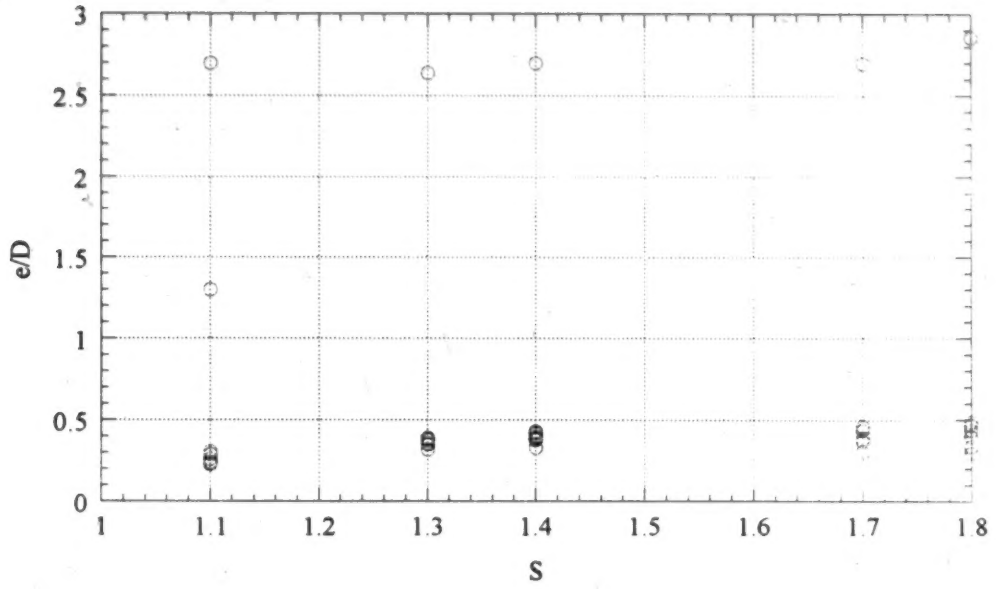

Figure 4.18 Normalized length scale "e/D" as a function of the spacing parameter S (Including RS5-S/S', d=1.2 cm)

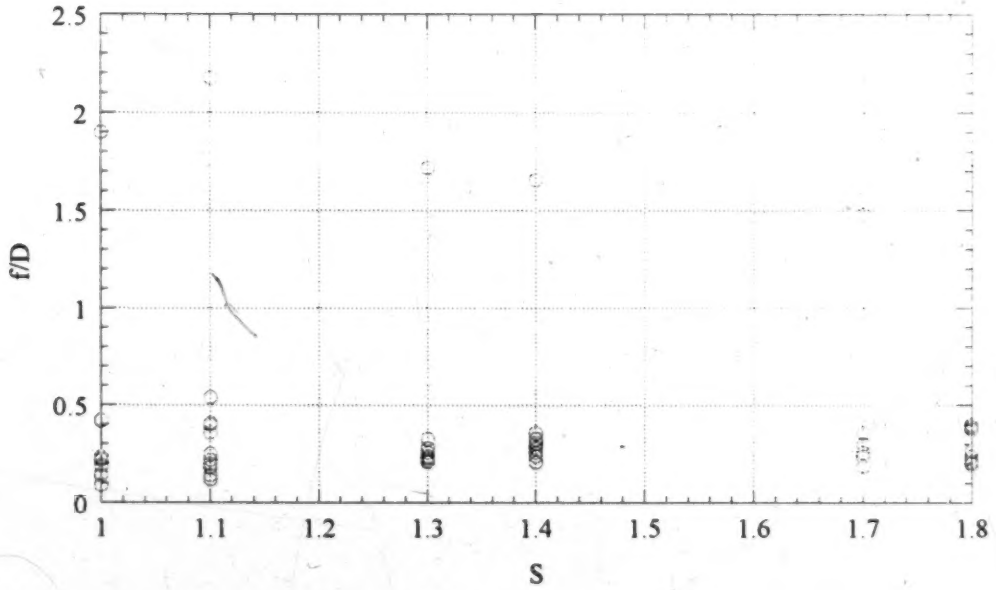

Figure 4.19 Normalized length scale "f/D" as a function of the spacing parameter S (Including RS5-S/S', d=1.2 cm)

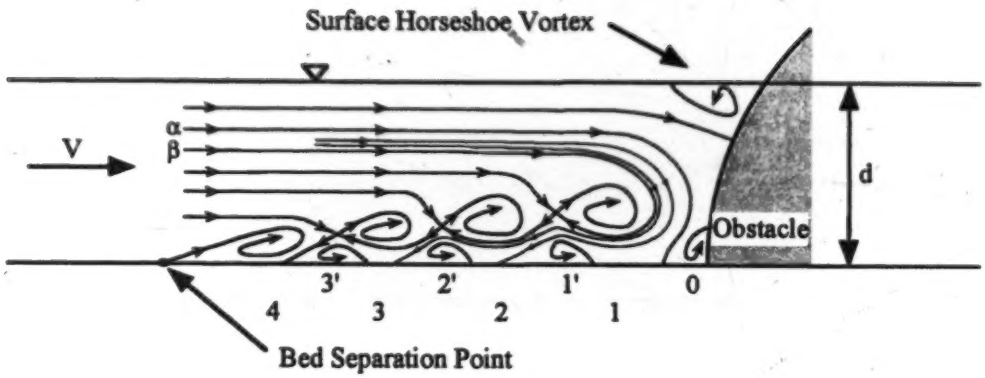

(a)

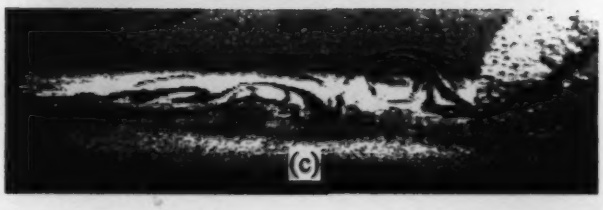

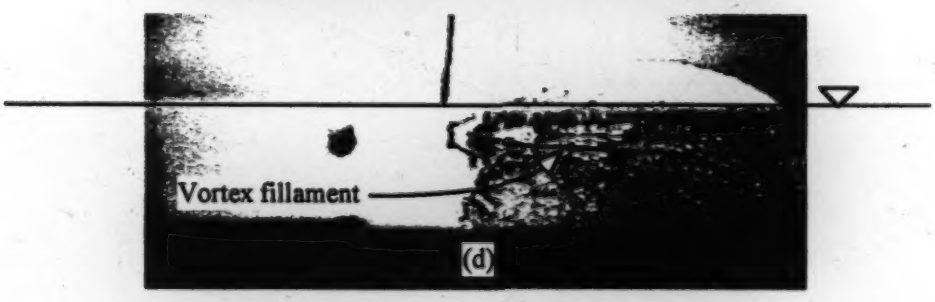

Figure 4.20 Horseshoe vortex cascade - side view

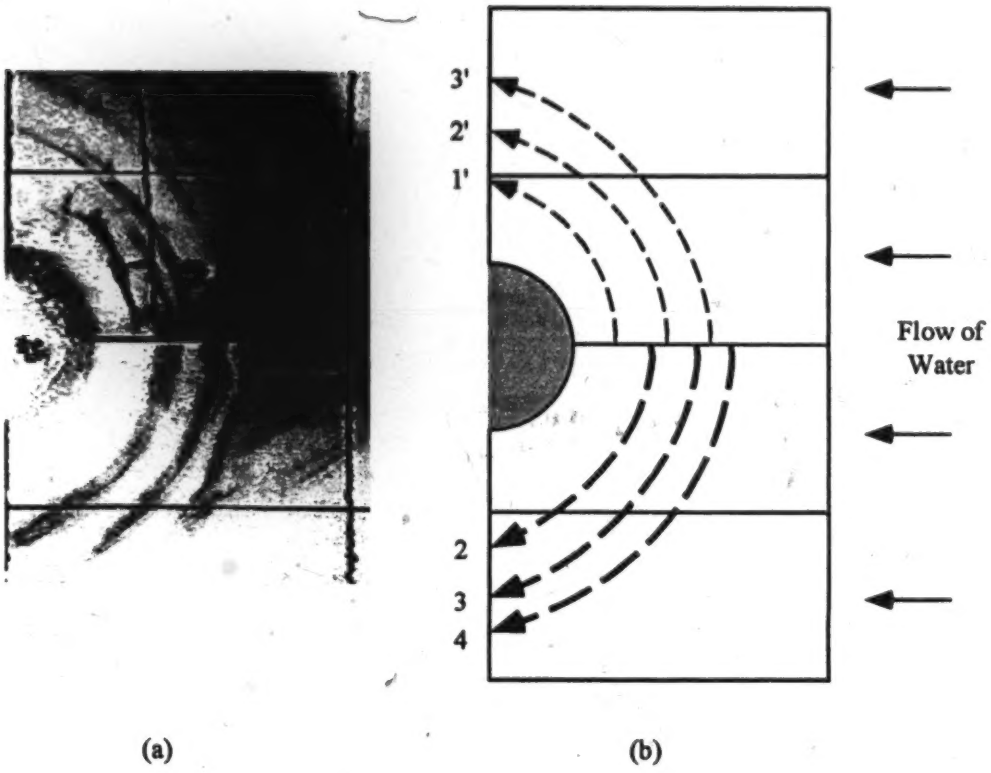

Figure 4.21 Horseshoe vortex cascade - plan view

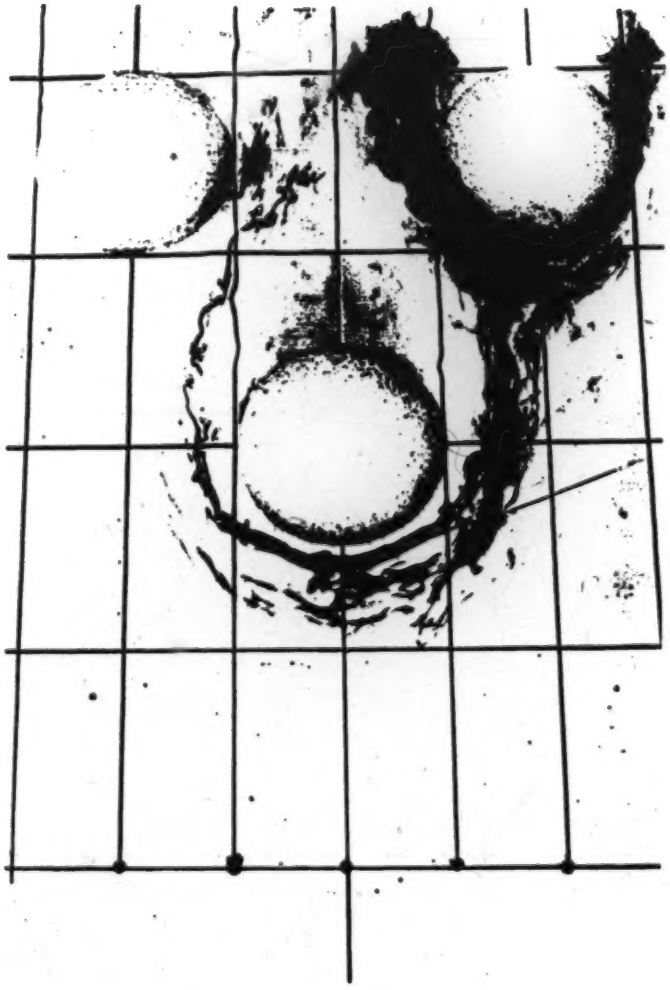

Figure 4.22 LE vortex filaments deflected between TEs

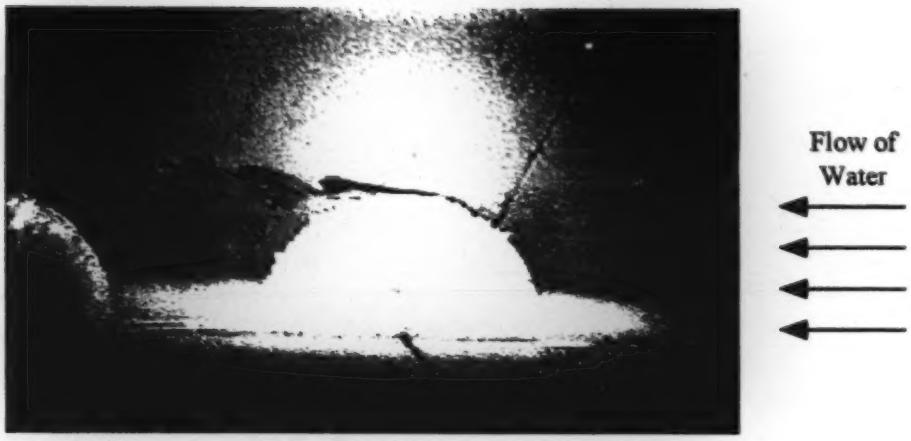

Figure 4.23 Arch vortex shedding from LE when S/S' ≥ 1.7/1.8

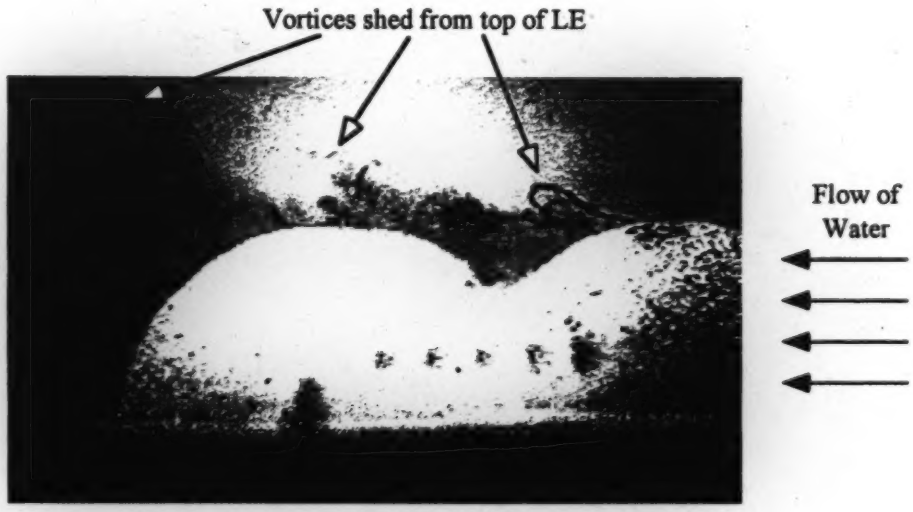

Figure 4.24 Arch vortex shedding from LE when S/S' < 1.7/1.8

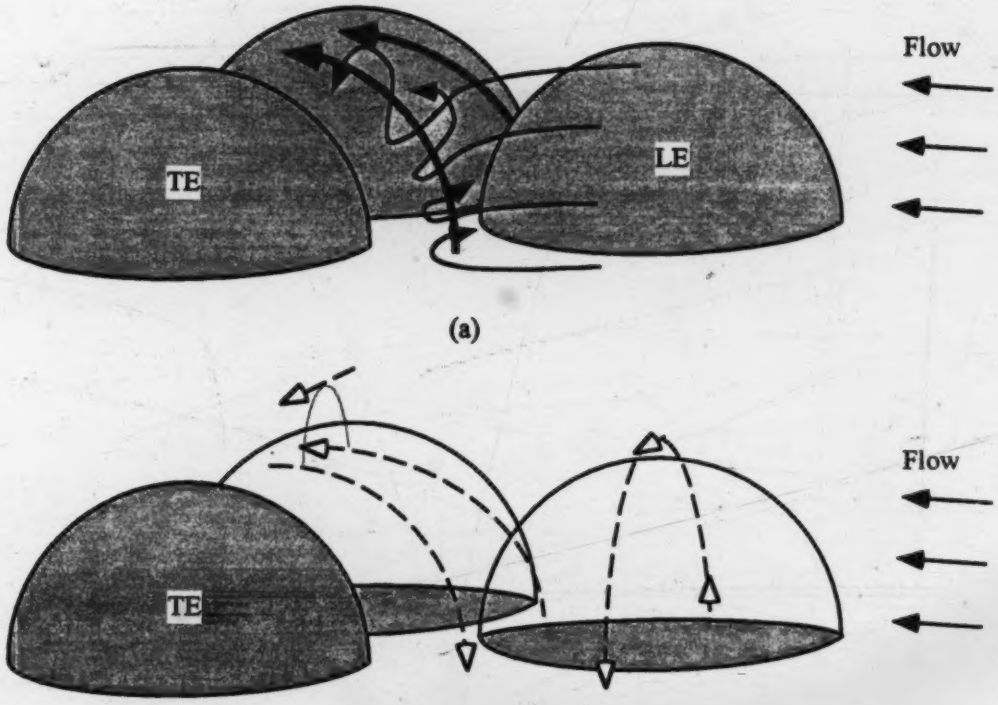

Figure 4.25 Schematic of arch vortex shedding from LE when S/S' < 1.7/1.8

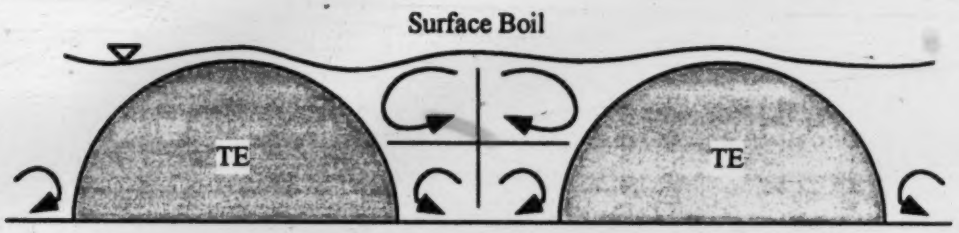

Figure 4.26 Vortex systems between TEs producing a surface boil

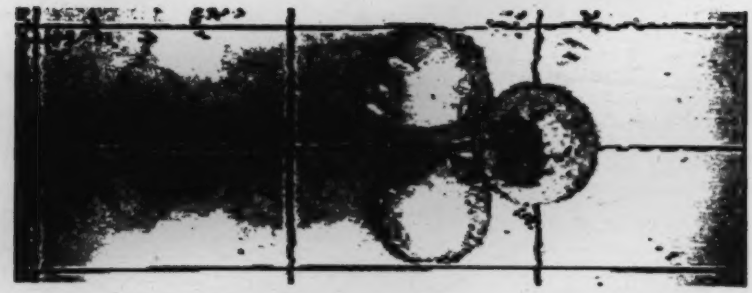

(a)

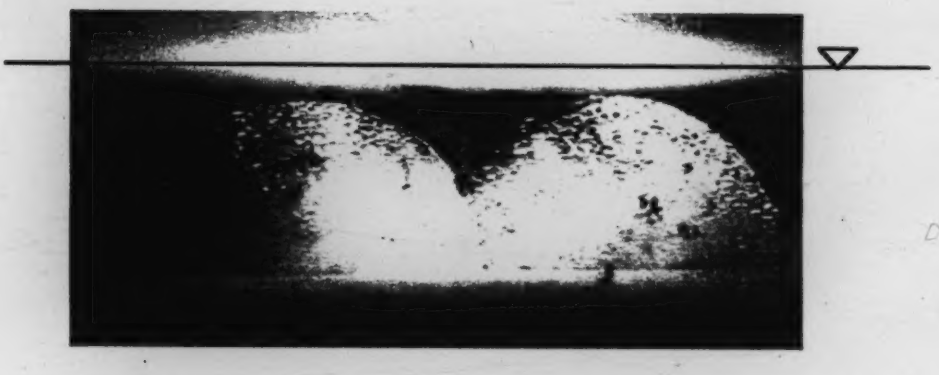

(b)

Figure 4.27 Fluid separation behind LE with small spacing

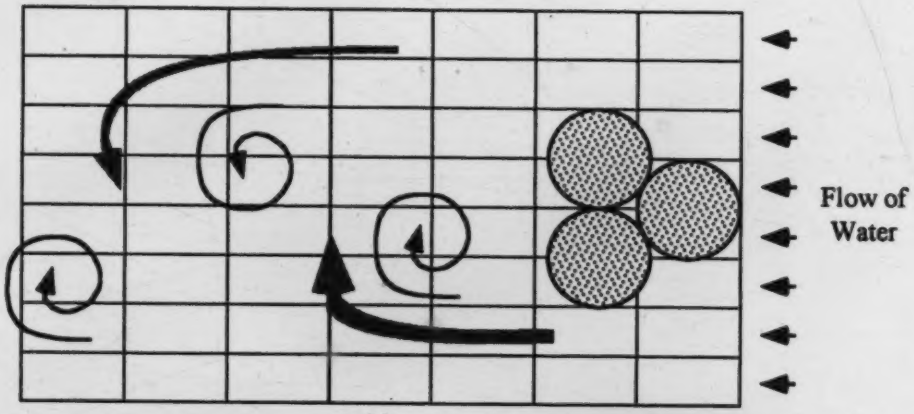

(a)

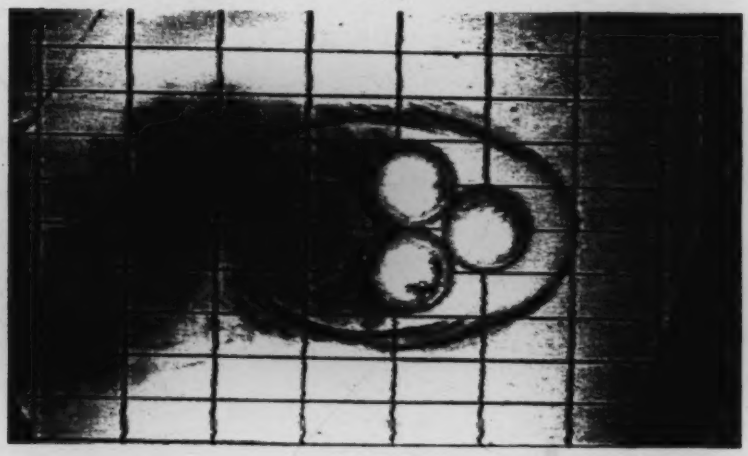

(b)

Figure 4.28 Asymmetrical vortex shedding

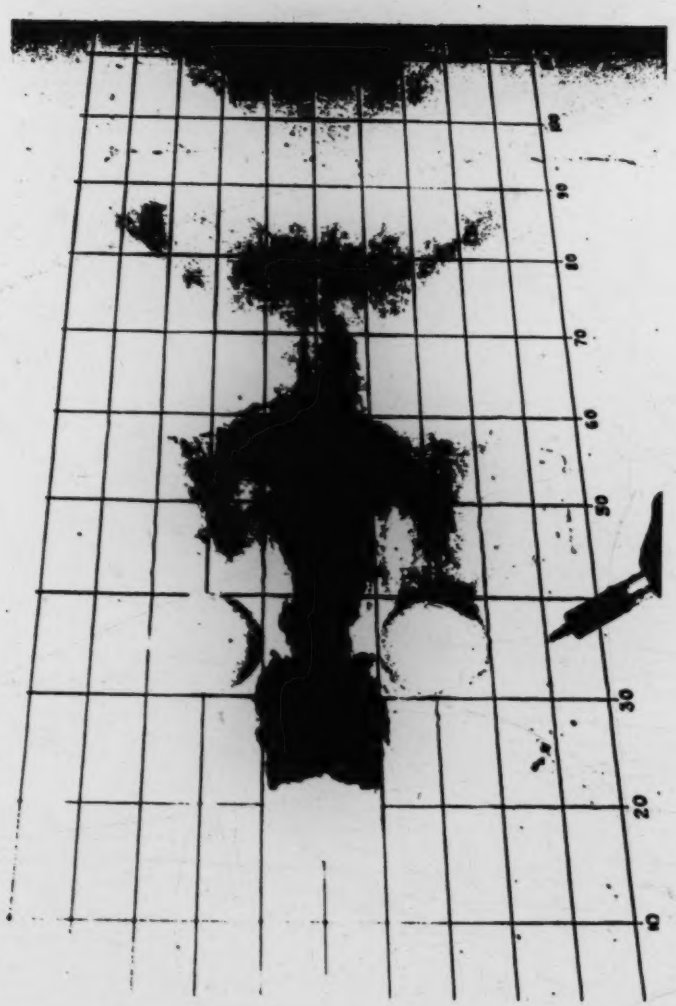

Figure 4.29 Symmetrical vortex shedding from the obstacle cluster

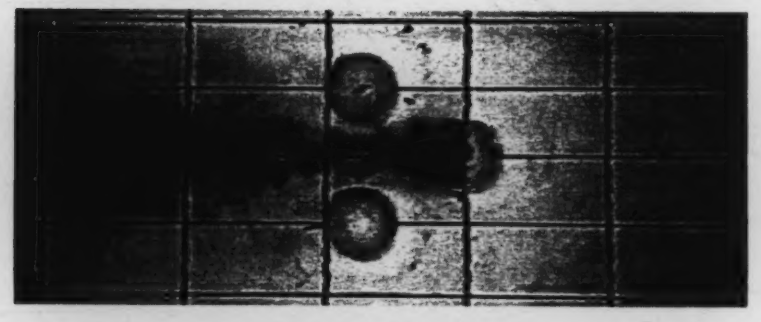

Figure 4.30 Independent obstacle wakes

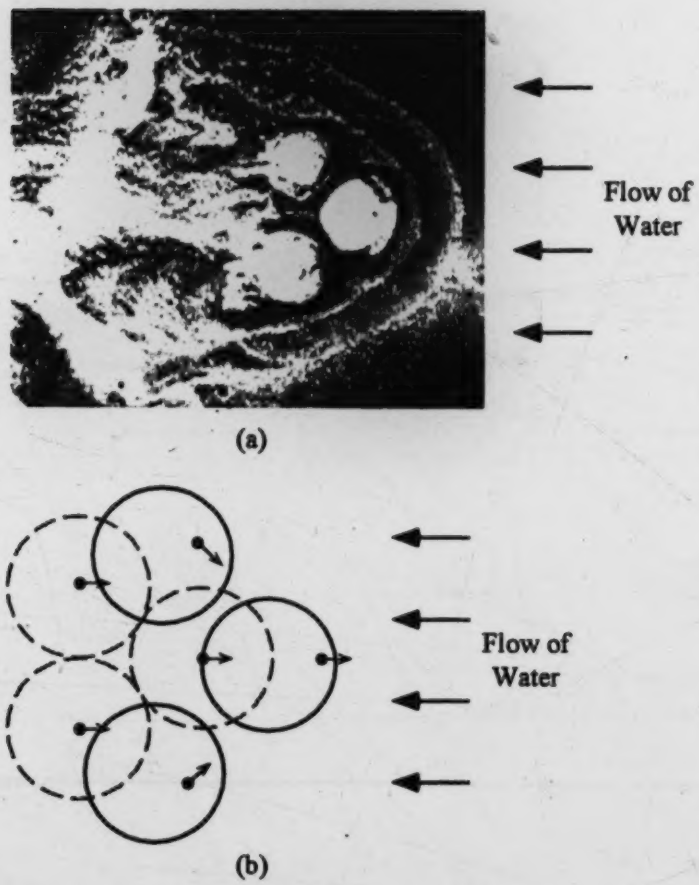

Figure 4.31 Movement of cluster placed on a mobile bed

CHAPTER 5

DISCUSSION

5.1 Major Findings

5.1.1 Depth of Flow

5.1.1.1 Bed Shear Profile Images

As stated in Section 4.2.1, the dye streaks contained in the images of Appendix B describe the orientation of the bed shear vector over a large area around the cluster. If we disregard local pressure effects of the cluster, changes to the direction of the bed shear vector in an open channel flow are a boundary layer reaction to changes in the gradient of the water surface. It is a characteristic of a Froudian dominated flow that the water surface gradient will be influenced by the obstacle being considered. This influence on the water surface gradient extends for many times the diameter of an obstacle in rivers since most natural flow conditions are gradually varied. A Reynolds dominated flow will influence the direction of the bed shear vector at a much smaller distance from the cluster than a Froudian flow.

The bottom two images ($d/h \leq 1.0$) in Figures B1 to B12 show significant changes to the bed shear vector at distances exceeding 3 obstacle diameters from the cluster. Additionally, all the images ($d/h \leq 1.5$) in Figures B13 to B15 show extended effects to the bed shear vector. This observation is consistent with Froudian flows. The top two images ($d/h \geq 2.0$) in Figures B1 to B12 do not display significant effects to the bed shear vector at distances removed from the cluster exceeding 1 obstacle diameter. This finding confirms the assumption of Reynolds flow around the obstacles at larger relative depths

The diameter of the obstacle and the relative depth of flow respectively are $D = 5$ cm and $d/h = 0.5$ for the bottom left images in Figures B7 to B12. In these images, the bed shear

vector is profoundly affected by the presence of the cluster. This observation also confirmed the assumption of Froudian flows for small relative depths however, it was discovered that under these conditions the flow in the flume was laminar (R = 708). The vortex cascade illustrated in Figure 4.20a occurred under these conditions. Due to the unique vortex patterns generated, general discussion of flow phenomenon in later sections will exclude this set of experiments unless otherwise stated.

5.1.1.2 Separation Profile Images

Examination of the images in Appendix A reveals a significant general local flow pattern that depends on d/h. Let us take the set of experiments where D = 10 and S/S' = 1.3/1.4 in Figure A4 as an illustrative example . The general outline of the separation line for the leftmost image in this four image series is relatively smooth around the entire cluster. This smooth outline indicates that the flow is being diverted around the cluster. The flow encountering the TE is thus highly influenced by the presence of the LE. As d/h increases the general shape of the separation line is more distinctly associated with each individual obstacle rather than with the entire cluster. The LE separation line is 'tucked' in behind the LE which indicates that the fluid is being drawn in behind the LE instead of being diverted around the cluster as in the low relative depth. A similar pattern is exhibited by most of the other experimental series. This pattern indicates that the flow encountered by the TE for larger relative depths is not affected as much by the presence of the LE as it is when the relative depth is small.

5.1.1.3 Separation Profile Plots

The parameter a/D is plotted vs. d/h in Figure 4.2. In this figure there can be observed a slight tendency for a/D to decrease as d/h increases. A possible explanation for this trend may be that flows with higher relative depths will contain more energy in turbulence. The more energetic turbulence in these flows suppresses separation from the bed since more

energy can be supplied to the boundary layer. Parameter b/D is plotted vs. d/h in Figure 4.3. A sensitivity to flow depth in the form of data scatter can be seen for d/h ≤ 1.0 in the figure. A similar behavior can be seen for parameter f/D in Figure 4.6. No significant trend can be noticed in the plot of e/D vs. d/h (Figure 4.5).

If we consider all the experiments where the parameter c/D exists (S/S' ≥ 1.7/1.8) then a strong tendency for c/D to decrease as d/h increases can be seen in Figure 4.4. This relationship is consistent except for the single rogue point associated with the 10 cm diameter hemisphere that was measured when d/h = 3.0. The parameter c/D is an inverse parameter that describes the distance of the TE separation line from the LE. An increase in c/D means that the flow is separating closer to the TE. It is unclear how this trend is significant.

The data plotted in Figures 4.12 to 4.19 indicate that the values of the length parameters a/D, b/D, e/D and f/D when D = 5 cm and d/h = 0.5 are many times the values for all other experiments. These graphs do illustrate an extreme flow condition that is dependent on d/h. This flow condition also provided an excellent opportunity for flow visualization of localized vortex systems.

5.1.1.4 Wake of Obstacles

Regions of backflow in the wake of an obstacle cluster were significant when d/h = 0.5 Behind the cluster when d/h = 0.5 for each of the Appendix B images, regions of backflow extend for several obstacle diameters behind the cluster. The regions of backflow behind the obstacles were often not symmetrical in the images contained in Appendix B and this is due to the fact that the cluster produced a Karman vortex street. Thus the backflow shifted from side to side in a cyclical manner. The region of backflow was significantly reduced when the relative depth was d/h = 1.0.

A Karman vortex street (Figure 4.28) was observed to form behind the cluster when d/h = 0.5 regardless of the spacing of the obstacles. This series of shed vortices is known to develop as a 2-D flow feature behind a single obstacle to the flow. Thus the wake of the cluster can be assumed to behave as a 2-D flow and the cluster can be assumed to behave as a single large obstacle to the flow. This is significant because at a spacing of S/S' = 1.8/2.0 the width of the cluster (outside of one TE to the outside of the other TE) is 3D. Thus three small obstacles can exhibit behavior similar to that of a virtual obstacle with a diameter three times that of the individual obstacles.

Asymmetrical vortex shedding when d/h = 1.0 (Figure 4.29) was not a common phenomenon and was very sensitive to small changes in flow conditions. It appeared to develop as a brief transition between the fully two dimensional flow associated with the Karman vortex street and the three dimensional flows associated with full submergence of the obstacles.

5.1.2 Obstacle Spacing

5.1.2.1 Separation Profile Images

It was expected that the SPs would provide the most significant insight into the dependence of flow behavior on the spacing of the obstacles. This is because the line of flow separation near the obstacles is a local effect of the cluster presence. The SP images contained in Appendix A reveal a significant change in bed separation patterns when considering only changes to the obstacle spacing (columns of images). The overall outline of the bed separation line becomes smoother as we view obstacles spaced closer together Furthermore, the bed separation line located directly in front of the TEs becomes faint and disappears as one moves from the images of larger spaced obstacles to those of smaller spaced obstacles. This was believed to be due to the fact that the LE HS vortex

was beginning to dominate the HS vortex in front of the TE. The dominant LE HS vortex rapidly removes dye from the bed in front of the TE and the separation line disappears.

5.1.2.2 Bed Shear Profile Images

The most significant information we can obtain from the BSP images regarding the spacing of the obstacles in the cluster is that the stagnant fluid immediately behind the TEs is charged with momentum as the obstacle spacing increases. When the obstacles are touching each other and d/h = 0.5 (bottom two images in Figures B1 and B7) then the obstacle cluster behaves as a complete obstruction to the flow and fluid behind the TEs is approximately stagnant. Once there is a small space between the TEs (all Appendix B images except Figures B1 and B7) then there is a channel for fluid containing momentum to charge the wake. At large obstacle spacings there is no combined accumulation of stagnant fluid behind the TE and the region of backflow for the obstacles is similar to that described by Shamloo (1997) for single obstacles.

5.1.2.3 Separation Profile Plots

No significant relationship between a/D and S was found in Figure 4.7. This finding was expected since a/D is represents the dimensionless distance between the LE and the separation line. Changes to obstacle spacing should not be sensed by the flow on the upstream face of the LE.

The plots of b/D and f/D vs. S are contained in Figures 4.8 and 4.9. At moderate to large obstacle spacings ($S/S' \geq 1.3/1.4$), b/D and f/D show little sensitivity to obstacle spacing. At smaller obstacle spacings ($S/S' \leq 1.1/1.2$), both b/D and f/D show a significant sensitivity to spacing in the form of data scatter. Further examination of Figures 4.8 and 4.11 reveals that the values for b/D and f/D are nearly identical when $S/S' \geq 1.3/1.4$.

One of the strongest dependencies on obstacle spacing was displayed by c/D which did not have a value when S/S' ≤ 1.4.1.6 (Figure 4.9). When the parameter c/D is zero, this represents the point where a feature that is distinctly associated with the TE is in contact with the LE. The scatter present in Figure 4.9 is most likely due to the fact that the length scale c was typically very small. The value of c was never more than 10 times greater than the estimated error in measurement and was typically around 5 times the estimated error.

The data plotted in Figure 4.10 indicates that e/D is not sensitive to obstacle spacing for moderate or large spacings (S/S' ≥ 1.3/1.4). When S/S' = 1.1/1.2 the values of e/D tend to be smaller. This tendency may be due to the fact that the TE HS vortex is destabilized by the presence of the LE HS vortex. This destabilization of the TE HS vortex should permit the flow to separate closer to the TE. When S/S' = 1.0/1.0 a value for e/D does not exist since the TE has no separate HS vortex.

Data plotted in Figures 4.16 to 4.19 contain extreme values for each of the parameters a/D, b/D, e/D and f/D when D = 5 cm and d/h = 0.5. The characteristics of the bed separation were scaled to the diameter of the obstacles D. Under the special hydraulic conditions D = 5 cm and d/h = 0.5 the cluster always behaved as a single obstacle to the flow. A more appropriate length scale for the bed separation characteristics under these conditions may be the width of the cluster from outside of TE to outside of TE.

5.1.3 Obstacle Size

It was expected that the size of the obstacle would have little effect on flow characteristics when proper modeling techniques are used. The technique of dividing an appropriate length scale by the obstacle diameter and restricting subsequent analysis to include only dimensionless parameters should remove any geometric dependency. This

was found to be the case when the non dimensional values of a/D, b/D, c/D, e/D and f/D plotted against d/h and S in figures 4.2 to 4.11. The scatter in the plots is believed to be more significantly associated with the measurement technique than with scaling the parameters to the obstacle diameter.

5.1.4 Mobile Bed Material

For the test where mobile bed material was used, there was no previous understanding of how the obstacle might behave. It was observed in Figure 4.31 that all of the obstacles shifted toward the scour hole that was developing around the obstacle cluster. This observed scour hole development was consistent with the findings of Fisher and Klingeman (1984). It was also observed that the scour hole which develops in front of the cluster is similar in shape to that created by a single obstacle. The deepest scouring occurred around the obstacles with little scouring at all between obstacles. This behavior is consistent with the findings of this study since this study indicated that obstacles that are touching should behave as a single obstacle to the flow. As the obstacles lean into the scour hole, their spacing increases. Hannah (1978) found that the interaction of piles in a pile group produces greater scour depths between the piles than would be created by a lone pile. If the spacing of the obstacles were to exceed S/S' = 1.1/1.2 then the results of this study indicate that the TEs should begin to develop HS vortices between them. These TE HS vortices may then increase the depth of scour between the obstacles. An increase in scour depth between obstacles should allow the obstacles to fall in toward each other thus reducing the obstacle spacing. The scouring between the obstacles may continue until $S/S' \leq 1.1/1.2$ at which time the cluster should again behave as a single obstacle to the flow.

5.2 Limitations of the Study

This study is somewhat limited due to the lack of validating field data. However since the study is investigative there was no prior understanding of what the most important features of the flow were. Field programs are costly and data are difficult to obtain without knowing what one is looking for. In this study the quantitative data (bed separation length scales) was used in an attempt to confirm the overall visual impression obtained from the images contained in Appendices A and B. The quantitative data were difficult to obtain with reasonable accuracy in a lab flume and would be very difficult to obtain from the field. Furthermore, any data that might have been obtained from the field would not be useful for validation purposes since differences in the bed geometry (HS vortex scour hole) would change the nature of the flow.

CHAPTER 6

CONCLUSIONS AND RECOMMENDATIONS

6.1 Conclusions

6.1.1 Depth of Flow

When the relative flow depth was small (d/h = 0.5), many significant features of the flow were observed. The direction of the bed shear vector was significantly deflected from streamwise at large distances from the cluster. Near to the cluster the LE tended to deflect flow away from the TEs. Two dimensional flow features such as the Karman vortex street formed behind the cluster. When Karman vortices were observed, the obstacle cluster behaved as a much larger virtual obstacle with a diameter equivalent to the distance between outer edges of the TEs. A large region of stagnant fluid was maintained behind the TEs. A cascade of up to 8 HS vortices formed in front of the cluster during the experiment where D = 5 cm. These conditions produced laminar flow. A single HS vortex also formed in front of the LE and immediately below the water surface during the experiments where D = 5 cm.

When the relative depth was d/h = 1.0, many of the previously observed flow features changed. The Karman vortices disappeared and an unstable two dimensional system of symmetrical vortices were observed to shed from the cluster. The large region of stagnant fluid behind the TEs was significantly reduced in size. A cascade of HS vortices was no longer observed.

When the relative depth was d/h $\geq$ 2.0, additional changes were observed to occur to the general flow features. The direction of the bed shear vector was not deflected significantly from streamwise at distances from the obstacle cluster greater than one

obstacle diameter. The flow did not tend to be deflected by the LE but instead went around the LE to more directly impact the TEs.

6.1.2 Obstacle Spacing

When the obstacle spacing was small ($S/S' \leq 1.1/1.2$), many significant flow features were observed. HS vortices did not form between the TEs and the LE HS vortex formed around the entire cluster. The stagnant region behind the TEs tended to be a continuous region as if created by a single obstacle. Fluid separation from the LE was reduced to a small area on the downstream side of the obstacle. Fluid separation from the TEs approximately bisected the obstacles.

When the obstacle spacing was moderate ($1.3/1.4 \leq S/S' \leq 1.4/1.6$), HS vortices did form between the TEs but were very unstable. The stagnant region behind the TEs was no longer shared by the TEs as a continuous region. A pair of vortices formed directly above and between the TEs when $d/h \geq 1.0$. These vortices were oriented parallel to the bed and their combined effect produced a strong vertical flow between them. Fluid separation from the LE did not occur at the base of the obstacle.

When the obstacle spacing was large ($S/S' \geq 1.7/1.8$), stable HS vortices formed in front of each of the obstacles. The fluid from the wake of each obstacle did not mix with any other obstacle wake except when the cluster shed large Karman vortices ($d/h = 0.5$). Fluid separation from the LE approximately bisected the obstacle.

6.1.3 Obstacle Size

The size of the obstacles was not found to have any influence on the general flow behavior when appropriate modeling techniques are applied.

6.1.4 Mobile Bed Material

Scouring of mobile bed material permitted closely spaced obstacles to increase their spacing by leaning into the scour hole created by the HS vortex. The spacing was not found to exceed (S/S' = 1.1/1.2) so that HS vortices were not permitted to form between TEs. Significant scouring did not occur between obstacles and overall scouring behavior was similar to that where a single obstacle was exposed to the flow.

6.2 Recommendations

6.2.1 Designs for Fish Habitat Structures

1. Complicated relationships between S and S' are not practical for design purposes therefore they should be considered equal.

2. The cluster always behaved as a single obstacle to the flow when the obstacle spacing was small (S/S' $\leq$ 1.1/1.2). Placement of obstacles in the field should therefore be such that the obstacles are approximately touching. This spacing of obstacles should eliminate any tendency for steady state scour between the obstacles to become larger than for a single obstacle.

3. Obstacles should be scaled to the seasonal depth of flow when habitat usage is most significant. If possible the obstacle diameter should not be less than twice the prime habitat depth of flow.

The above three recommendations may be considered valid only for hemispherical shaped obstacles with no angular protrusions from the surface.

6.2.2 Future Research

Future research goals may be to investigate the relationship between the geometry of a rock cluster placed on a mobile bed and the fluvial/hydraulic characteristics of a river. Attention may be paid to the differential movements of each element in a cluster and whether an initial cluster geometry would tend to "migrate" to an equilibrium geometry. Given that rocks placed as fish habitat may actually be highly angular rip rap, further research may be conducted on the influence of obstacle geometry/angularity within a cluster on overall cluster behavior.

REFERENCES

Ahmed, F., 1994, "Flow and Erosion Around Bridge Piers", Ph. D. Thesis, Department of Civil Engineering, University of Alberta, Canada.

Baker, C. J., 1979, "The Laminar Horseshoe Vortex", Journal of Fluid Mechanics, Vol. 95, Part 2, 347-367.

Baker, C. J., 1980, "The Turbulent Horseshoe Vortex", Journal of Wind Engineering and Industrial Aerodynamics, 6, 9-23

Department of Fisheries and Oceans, 1986, "Policy for the Management of Fish Habitat", Government of Canada, Ottawa, Ontario, Canada.

Fisher, A. C. and Klingeman, P. C., 1984, "Local Scour at Fish Rocks", pp. 286-290 in Schreiber, D. J., editor. "Water for Resource Development". Proc. American Soc. Civ. Eng, Hydraulics Division, Inland Empire Section, Coeur d'Alene, Idaho.

Hannah, C. R., 1978, "Scour at Pile Groups", M. Sc. Thesis, Department of Civil Engineering, University of Canterbury, Christchurch, New Zealand.

Lowe, S., 1992, "Fish Habitat Enhancement Designs: Typical Structures", Alberta Environmental Protection, Water Resources Management Services, Technical Services and Monitoring Division, River Engineering Branch.

Kellerhals, R., Neill, C. R. and Bray, D. I., 1972, "Hydraulic and Geomorphic Characteristics of Rivers in Alberta", River Engineering and Surface Hydrology Report 72-1, Alberta Cooperative Research Program in Highway and River Engineering, Edmonton, Alberta.

Okamoto, S., 1979, "Turbulent Shear Flow Behind a Hemisphere-Cylinder Placed on a Ground Plane", in: Turbulent Shear Flows 2, ed. by L. J. S. Bradbury, F. Durst, B. E. Launder, F. W. Schmidt, J. H. Whitelaw (Springer, Berlin Heidelberg New York) 171-185.

Okamoto, S., 1980, "Turbulent Shear Flow Behind a Sphere Placed on a Plane Boundary", in: Turbulent Shear Flows 2, ed. by L. J. S. Bradbury, F. Durst, B. E. Launder, F. W. Schmidt, J. H. Whitelaw, Springer, New York, 246-256.

Okamoto, T., 1977, "Flow Past Cone Placed on Flat Plate", Bulletin of the Jpn. Soc. Mech. Eng., Vol. 20, 329-336.

Potter, M. C. and Wiggert, D. C., 1991, "Mechanics of Fluids", Prentice Hall, Englewood Cliffs, New Jersey, USA.

Prandtl, L. and Tietjens, O. J., 1957, "Fundamentals of Hydro & Aeromechnaics", Dover, New York, New York, USA.

Rouse, H., 1963, "On the Role of Eddies in Fluid Motion", American Scientist, Vol. 51, 284-314.

R.L. & L. Environment Services Ltd., 1994, "Analysis of the Performance of Stream Habitat Structures in Southwestern Alberta", Data Report. Prepared for the Department of Fisheries and Oceans, Sustainable Fisheries Program in association with Alberta Environmental Protection, Fish and Wildlife Services. R.L. & L. Report No. 401F: 188 p. + App.

Shamloo, H., 1997, "Hydraulics of Simple Habitat Structures in Open Channels", Ph. D Thesis, Department of Civil Engineering, University of Alberta, Canada.

APPENDIX A

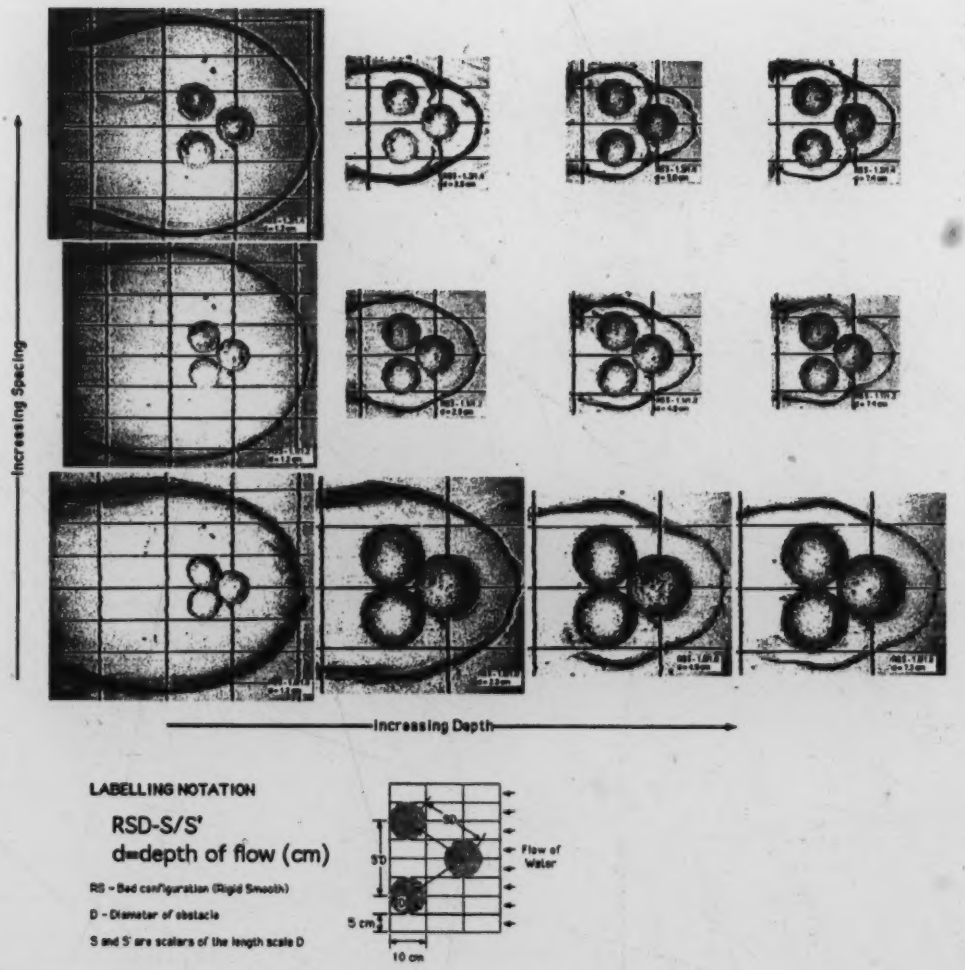

Figure A1. Composite SP, D = 5 cm, 1.3/1.4 ≥ S/S' ≥ 1.0/1.0.

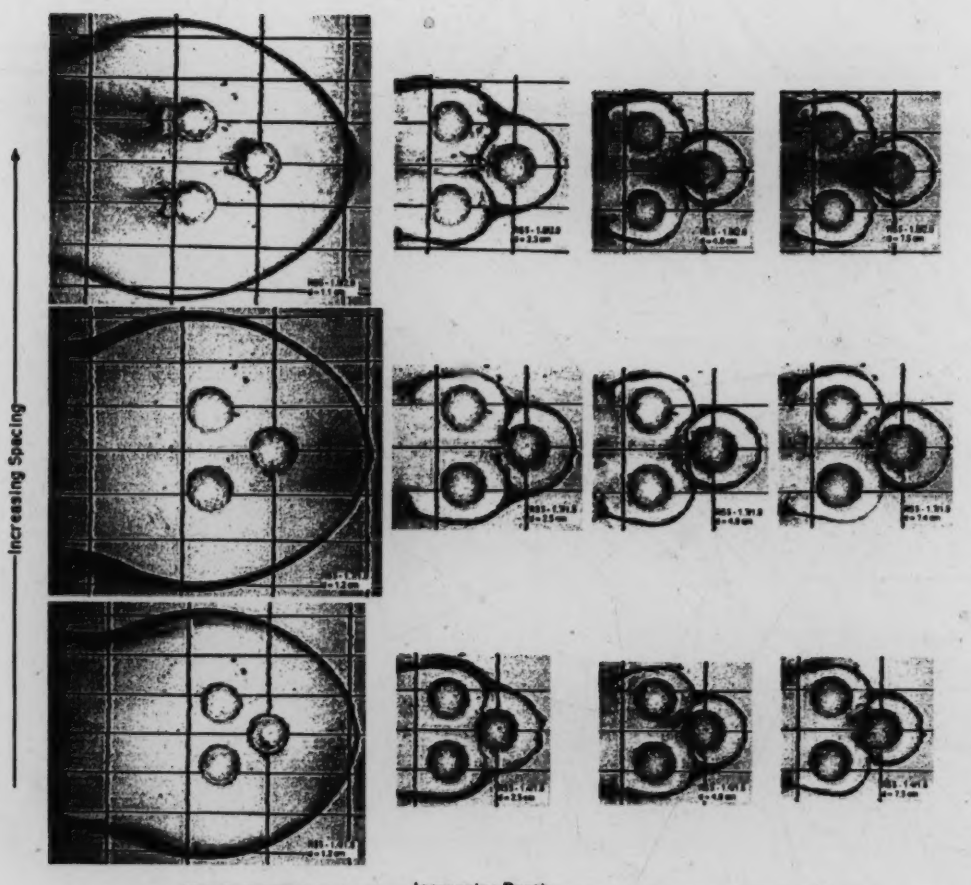

LABELLING NOTATION

RSD-S/S'

d=depth of flow (cm)

RS - Bed configuration (Rigid Smooth)

D - Diameter of obstacle

S and S' are scalars of the length scale D

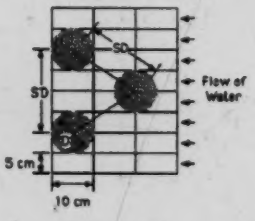

Figure A2. Composite SP, D = 5 cm, 1.8/2.0 ≥ S/S' ≥ 1.4/1.6.

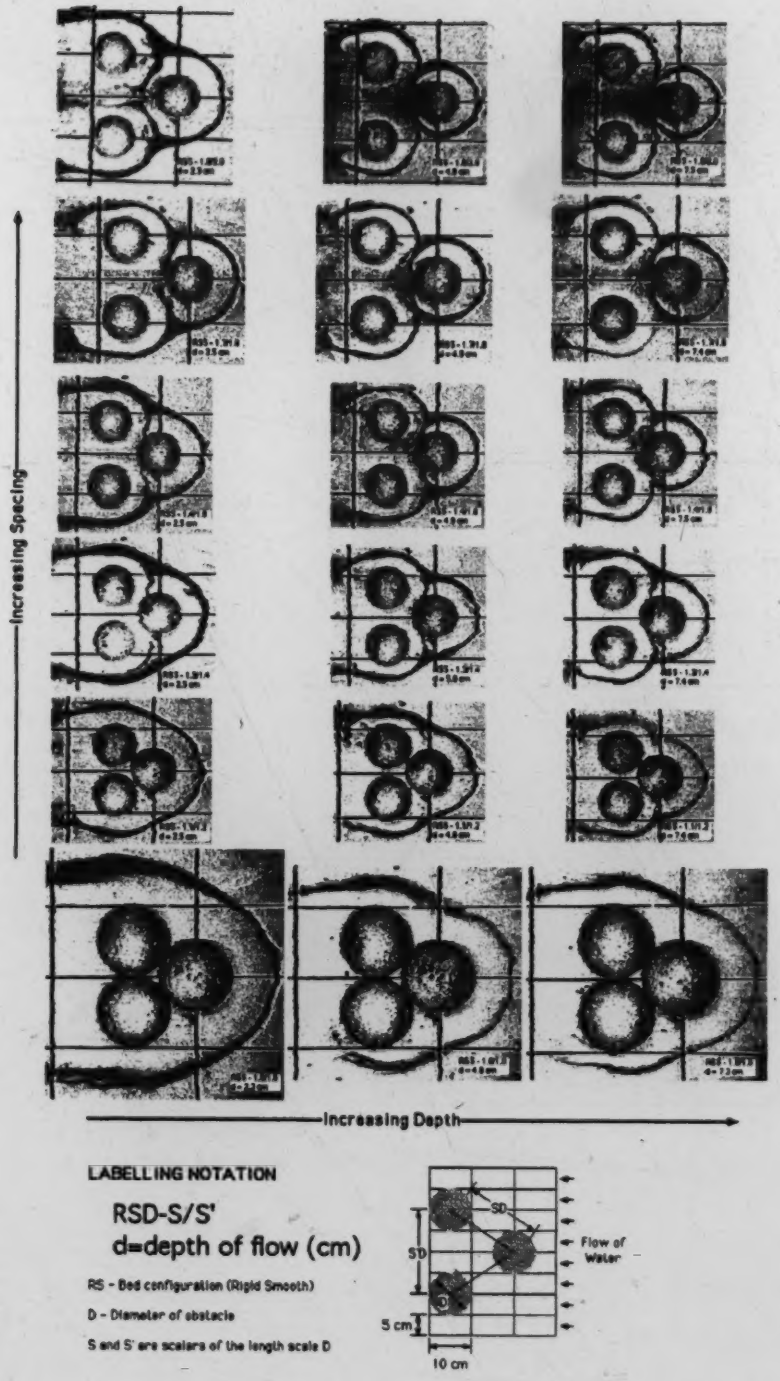

Figure A3. Composite SP, D = 5 cm, d≥h.

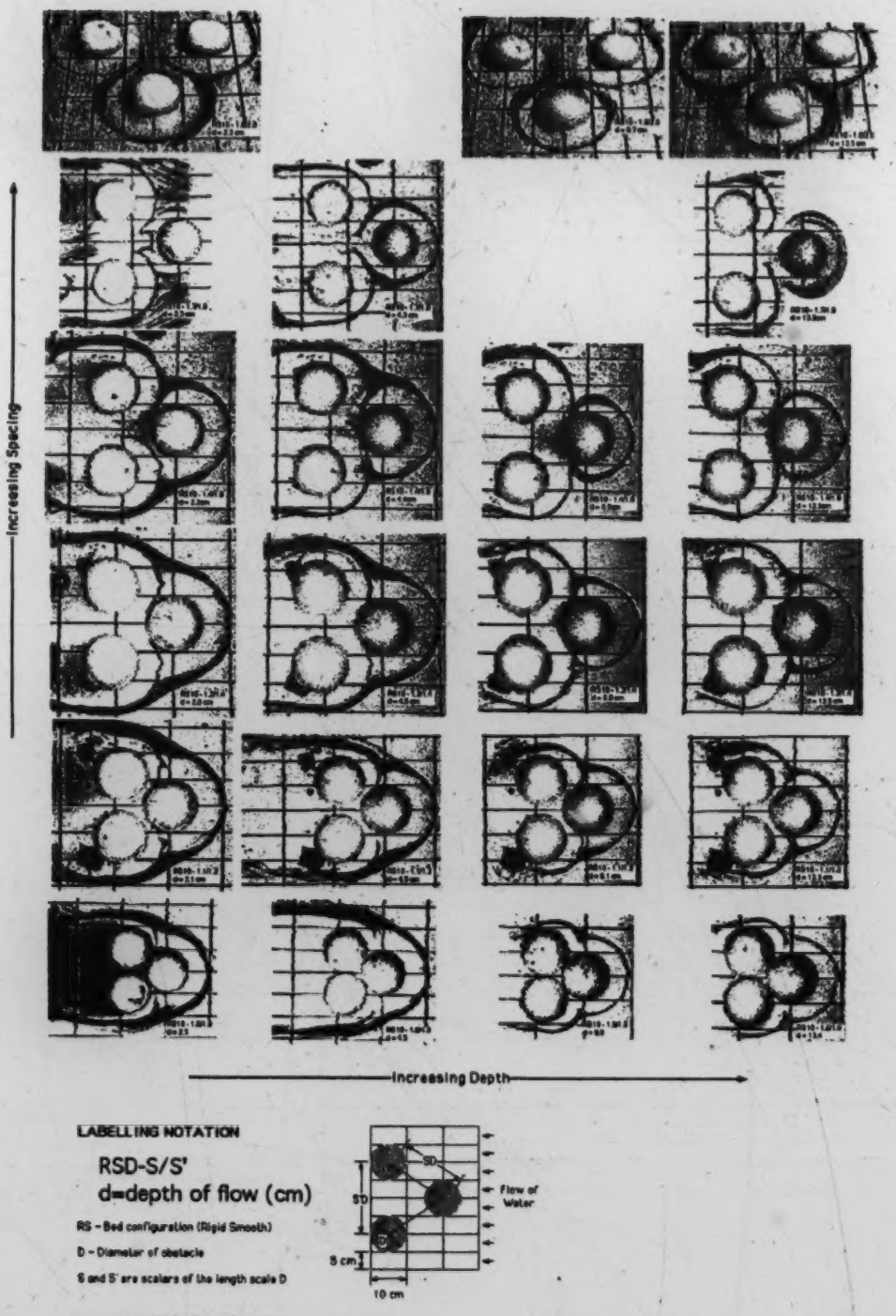

Figure A4. Composite SP, D = 10 cm.

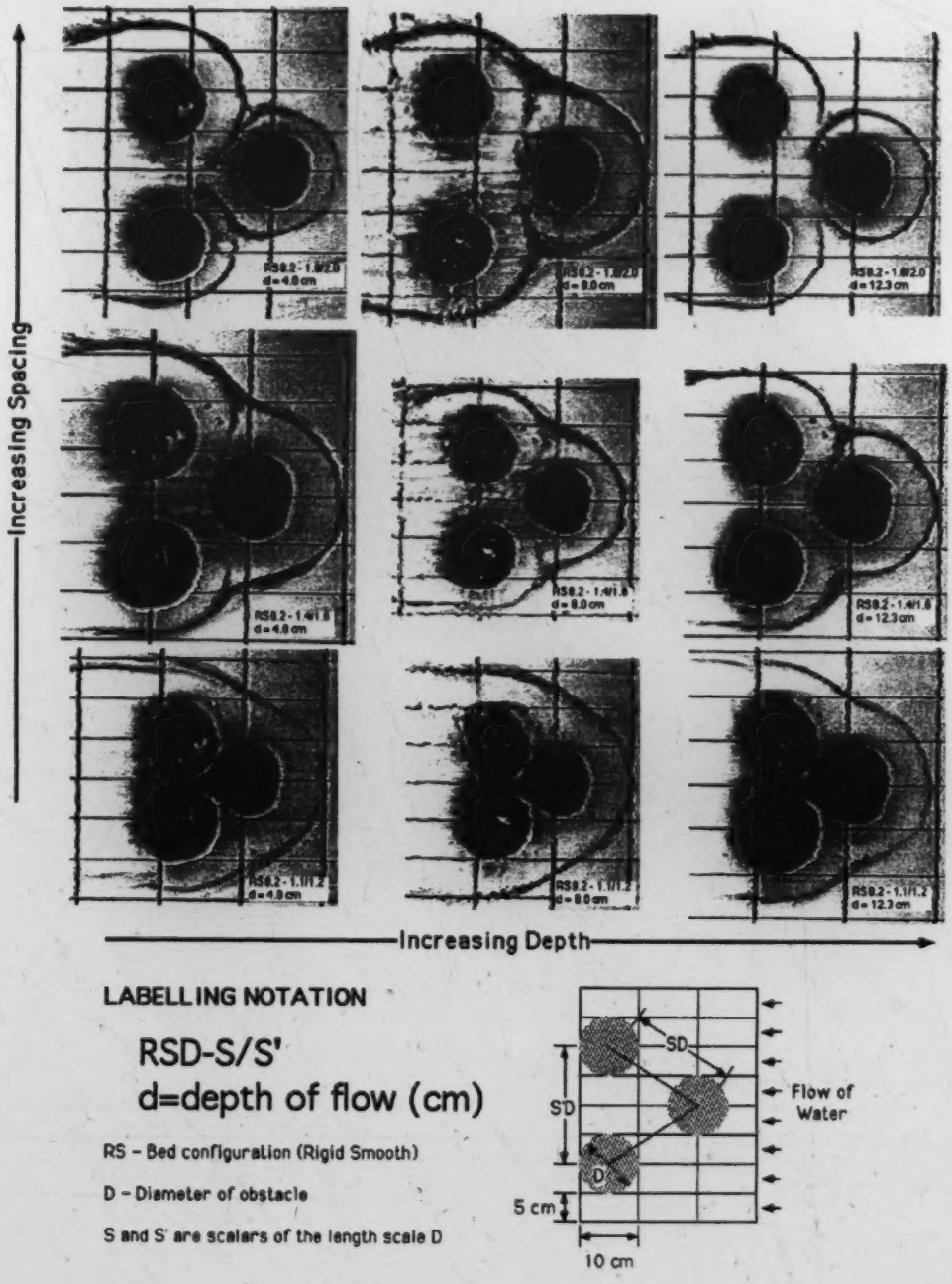

Figure A5. Composite SP, D = 8.2 cm.

APPENDIX B

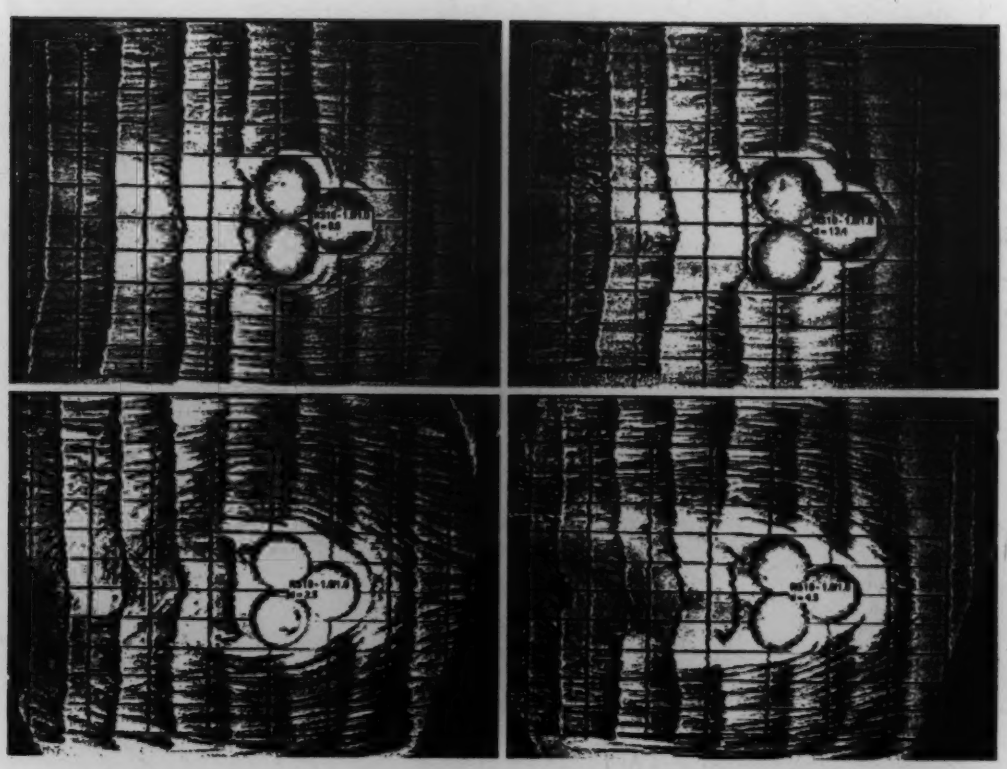

LABELLING NOTATION

RSD-S/S'
d=depth of flow (cm)

RS - Bed configuration (Rigid Smooth)

D - Diameter of obstacle

S and S' are scalars of the length scale D

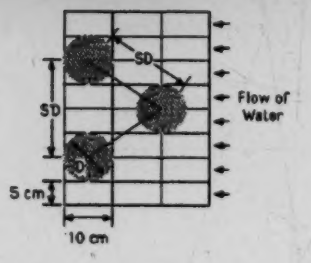

PICTURE ARRANGEMENT

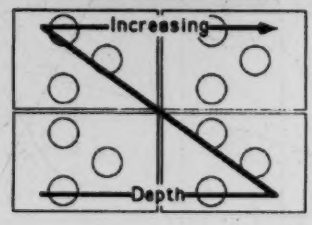

Figure B1. Composite BSP, D = 10 cm, S/S' = 1.0/1.0

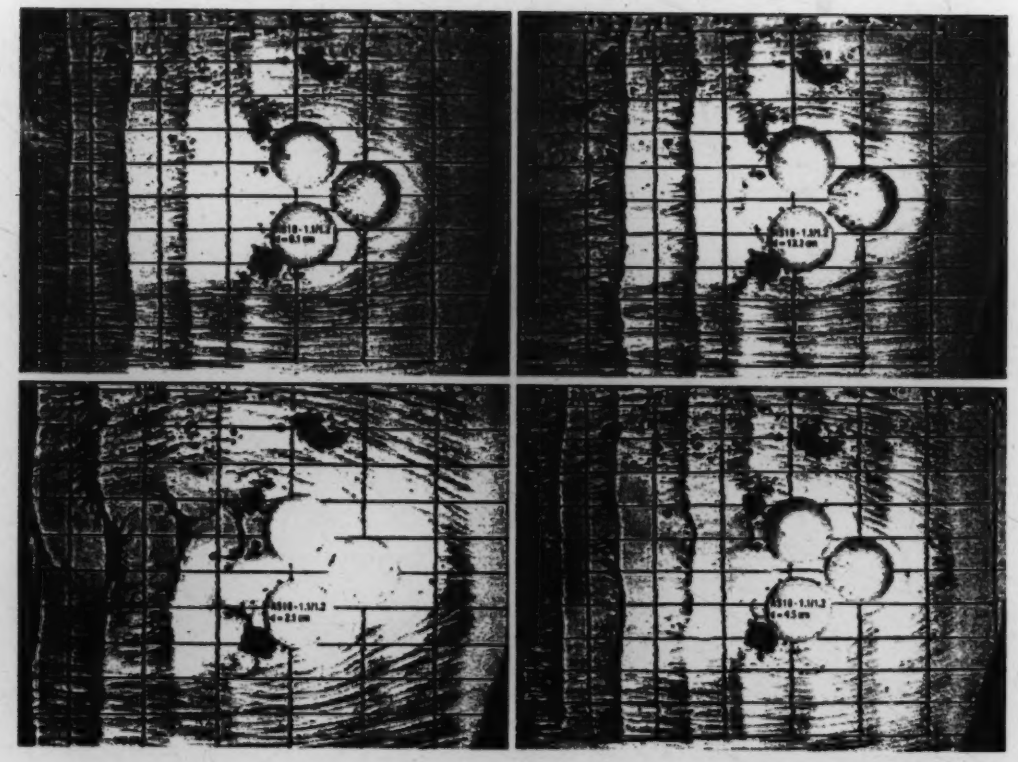

LABELLING NOTATION

RSD-S/S'
d=depth of flow (cm)

RS - Bed configuration (Rigid Smooth)

D - Diameter of obstacle

S and S' are scalars of the length scale D

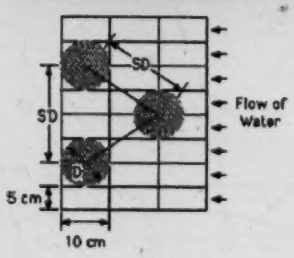

PICTURE ARRANGEMENT

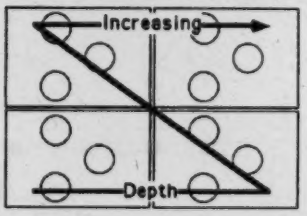

Figure B2. Composite BSP, D = 10 cm, S/S' = 1.1/1.2

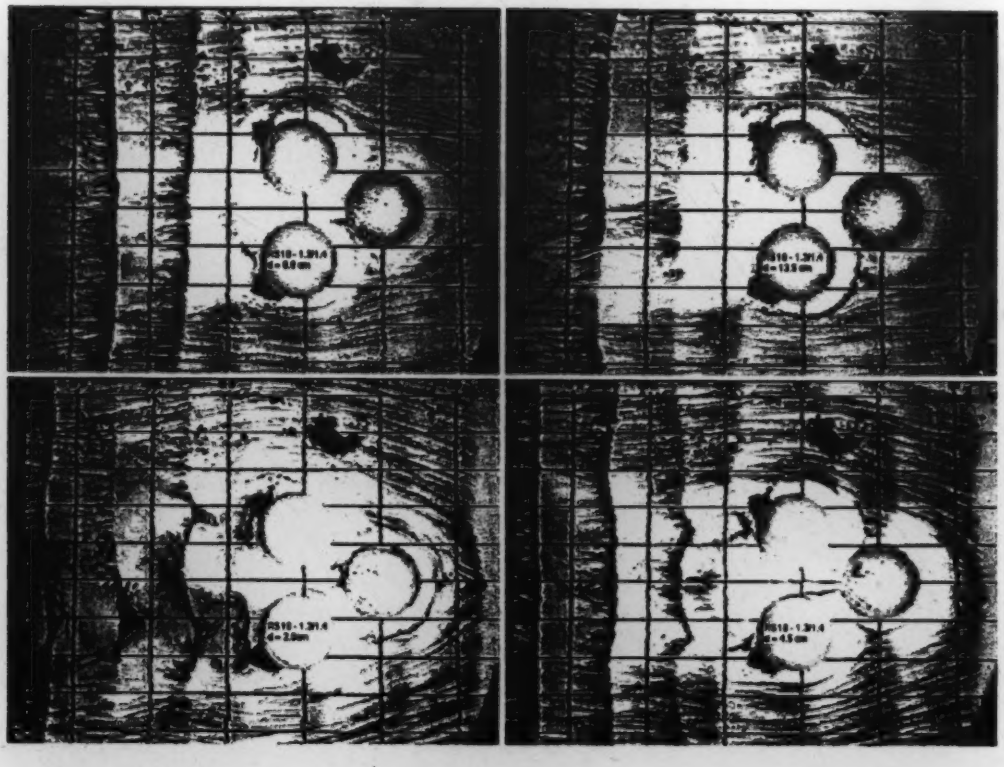

LABELLING NOTATION

RSD-S/S'
d=depth of flow (cm)

RS - Bed configuration (Rigid Smooth)

D - Diameter of obstacle

S and S' are scalers of the length scale D

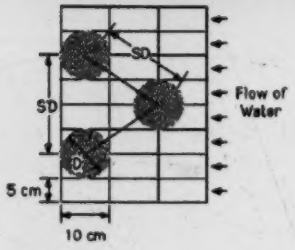

PICTURE ARRANGEMENT

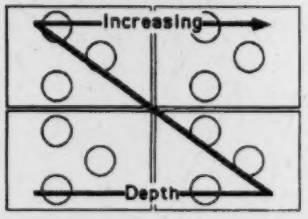

Figure B3. Composite BSP, D = 10 cm, S/S' = 1.3/1.4

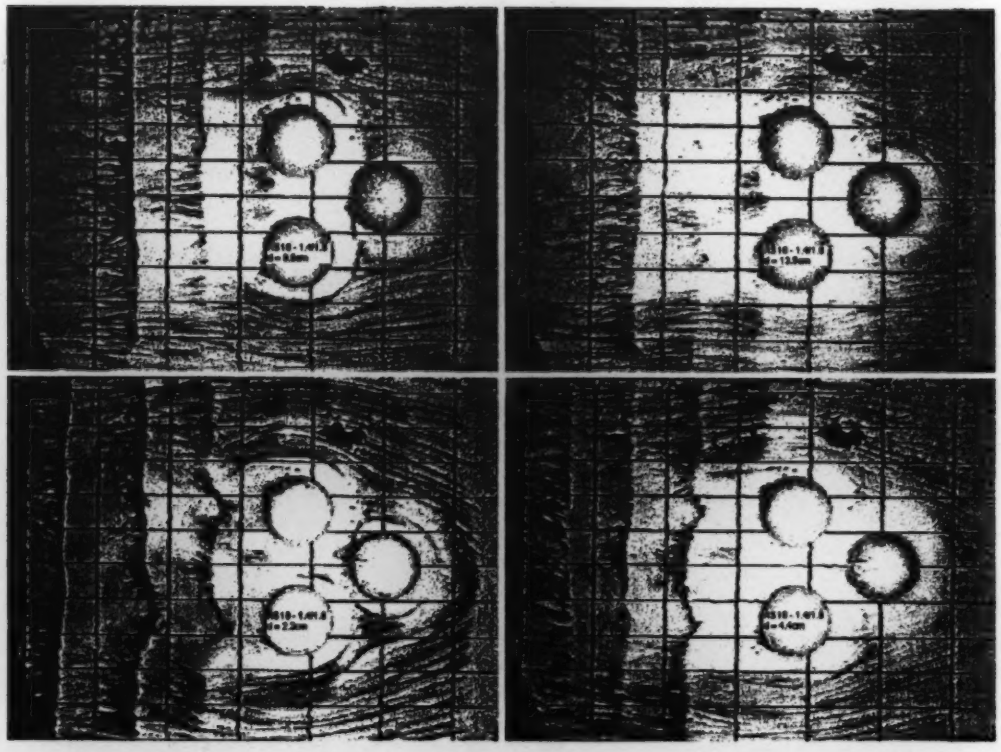

LABELLING NOTATION

RSD-S/S'
d=depth of flow (cm)

RS - Bed configuration (Rigid Smooth)

D - Diameter of obstacle

S and S' are scalars of the length scale D

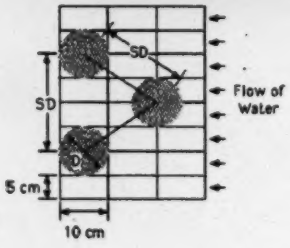

PICTURE ARRANGEMENT

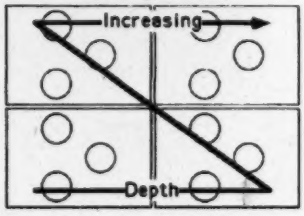

Figure B4. Composite BSP, D = 10 cm, S/S' = 1.4/1.6

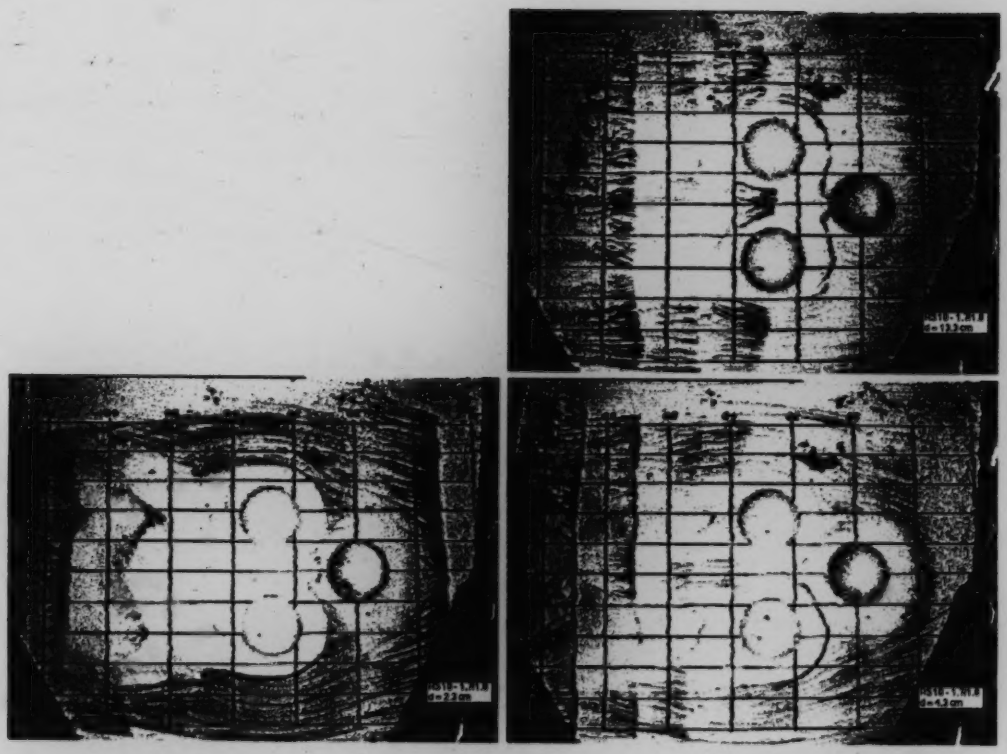

LABELLING NOTATION

RSD-S/S'
d=depth of flow (cm)

RS - Bed configuration (Rigid Smooth)

D - Diameter of obstacle

S and S' are scalars of the length scale D

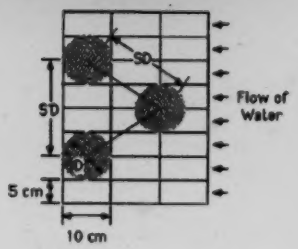

PICTURE ARRANGEMENT

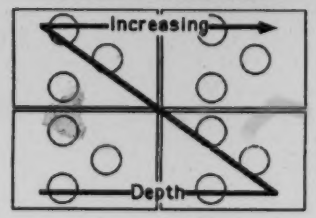

Figure B5. Composite BSP, D = 10 cm, S/S' = 1.7/1.8

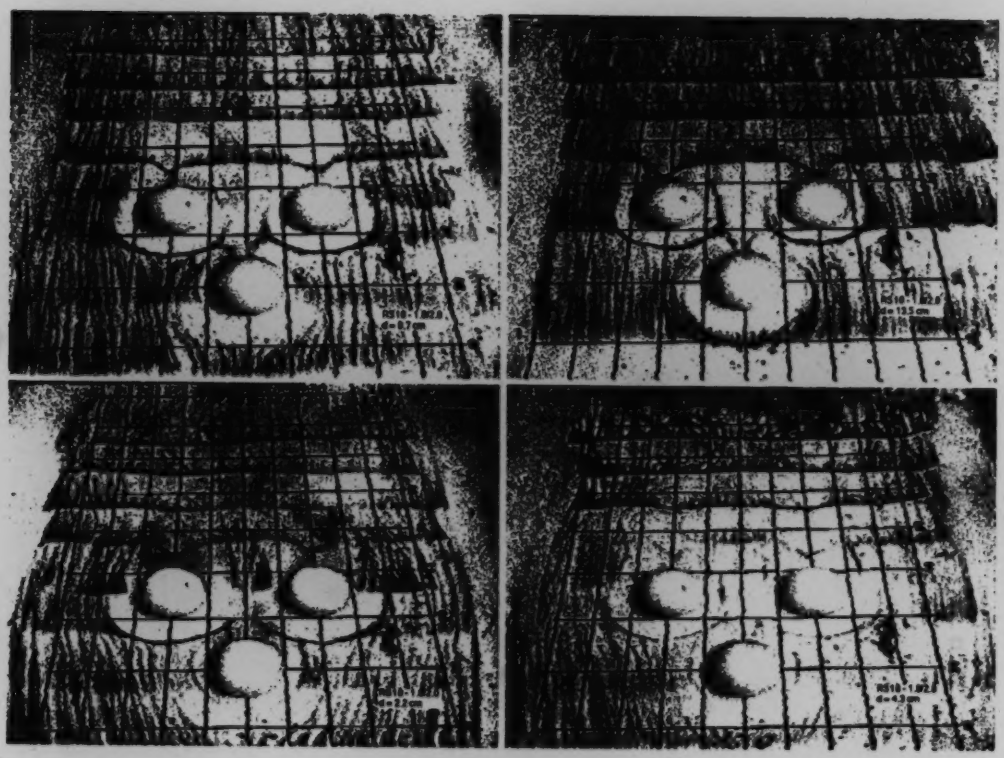

LABELLING NOTATION

RSD-S/S'
d=depth of flow (cm)

RS - Bed configuration (Rigid Smooth)

D - Diameter of obstacle

S and S' are scalars of the length scale D

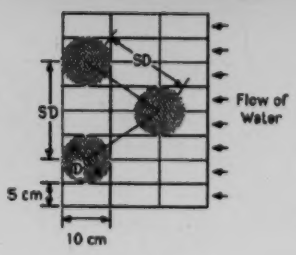

PICTURE ARRANGEMENT

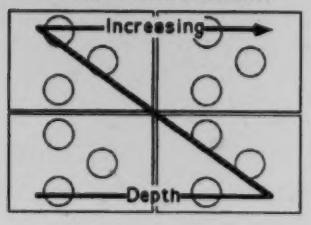

Figure B6. Composite BSP, D = 10 cm, S/S' = 1.8/2.0

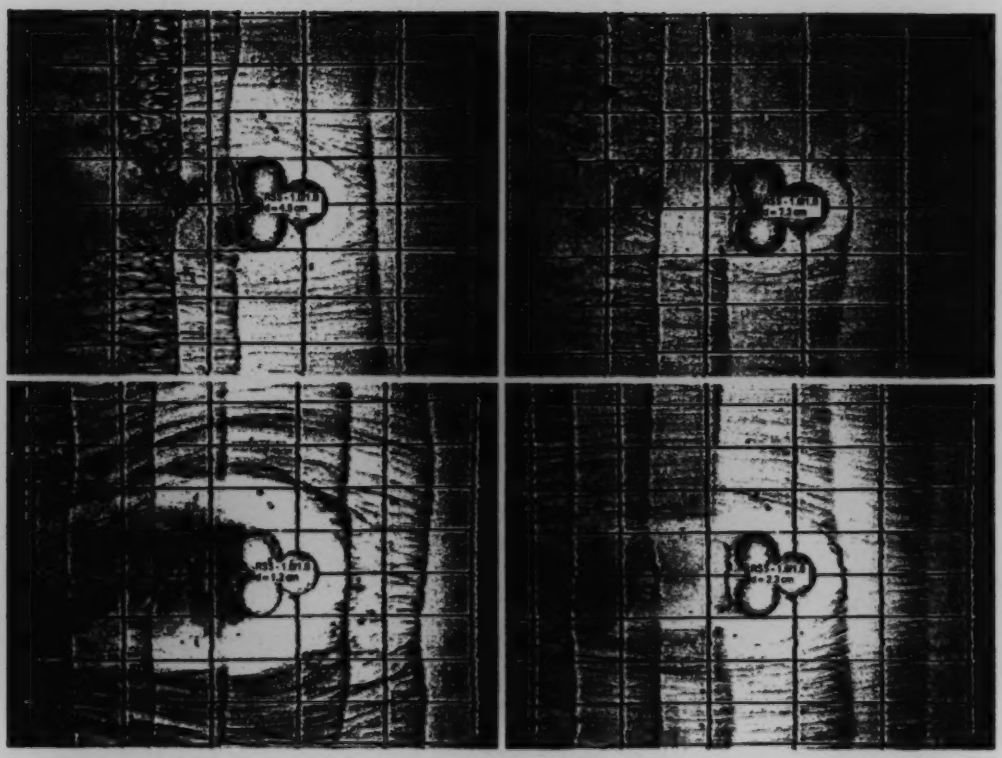

LABELLING NOTATION

RSD-S/S'
d=depth of flow (cm)

RS - Bed configuration (Rigid Smooth)

D - Diameter of obstacle

S and S' are scalars of the length scale D

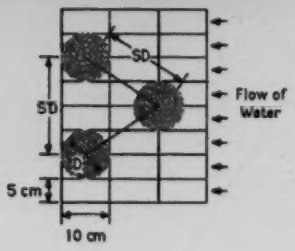

PICTURE ARRANGEMENT

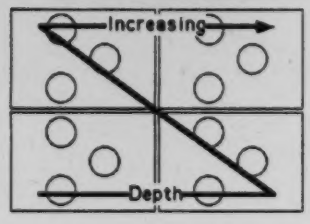

Figure B7. Composite BSP, D = 5 cm, S/S' = 1.0/1.0

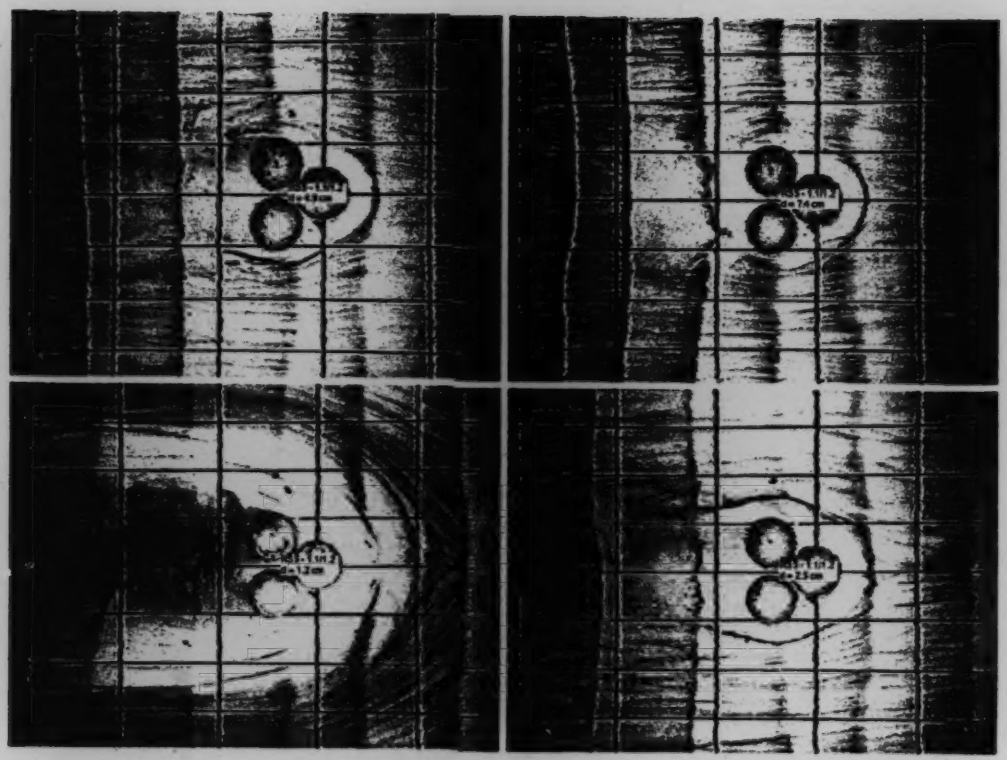

LABELLING NOTATION

RSD-S/S'
d=depth of flow (cm)

RS - Bed configuration (Rigid Smooth)

D - Diameter of obstacle

S and S' are scalers of the length scale D

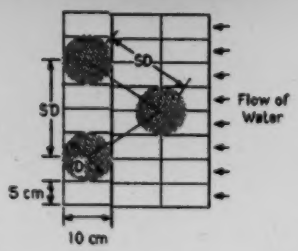

PICTURE ARRANGEMENT

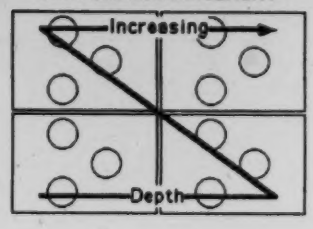

Figure B8. Composite BSP, D = 5 cm, S/S' = 1.1/1.2

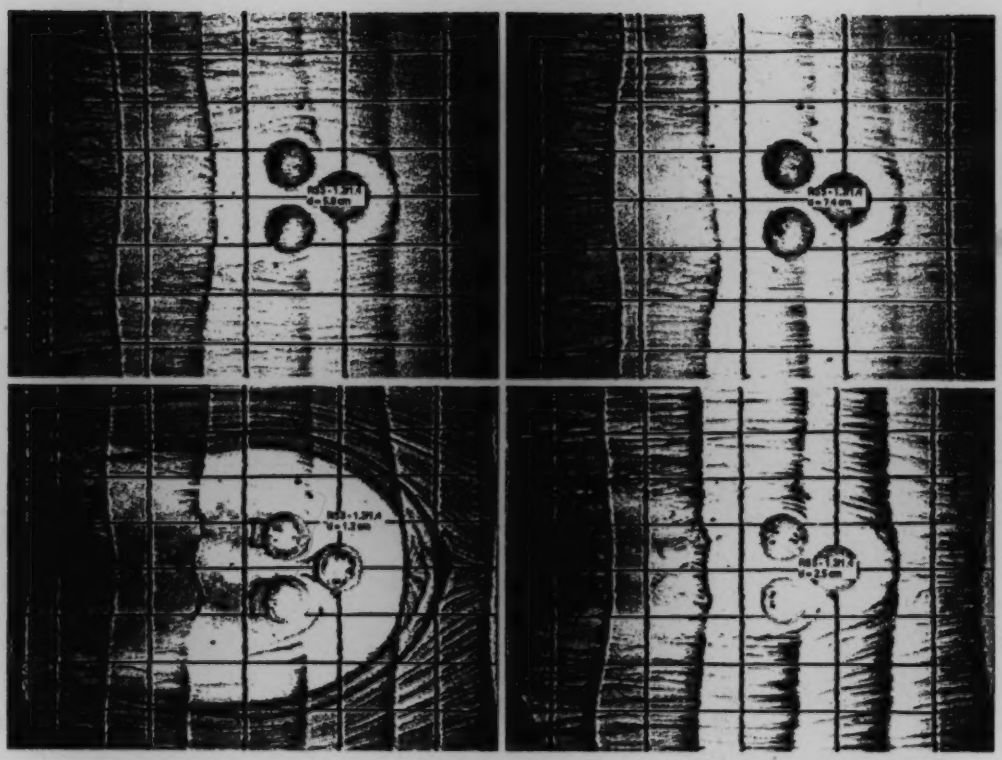

LABELLING NOTATION

RSD-S/S'

d=depth of flow (cm)

RS - Bed configuration (Rigid Smooth)

D - Diameter of obstacle

S and S' are scalars of the length scale D

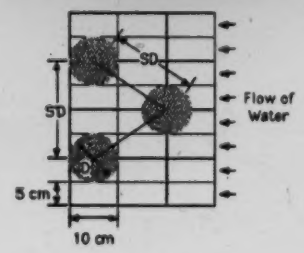

PICTURE ARRANGEMENT

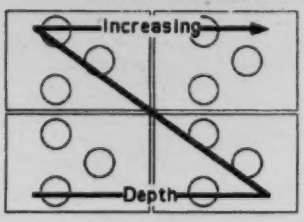

Figure B9. Composite BSP, D = 5 cm, S/S' = 1.3/1.4

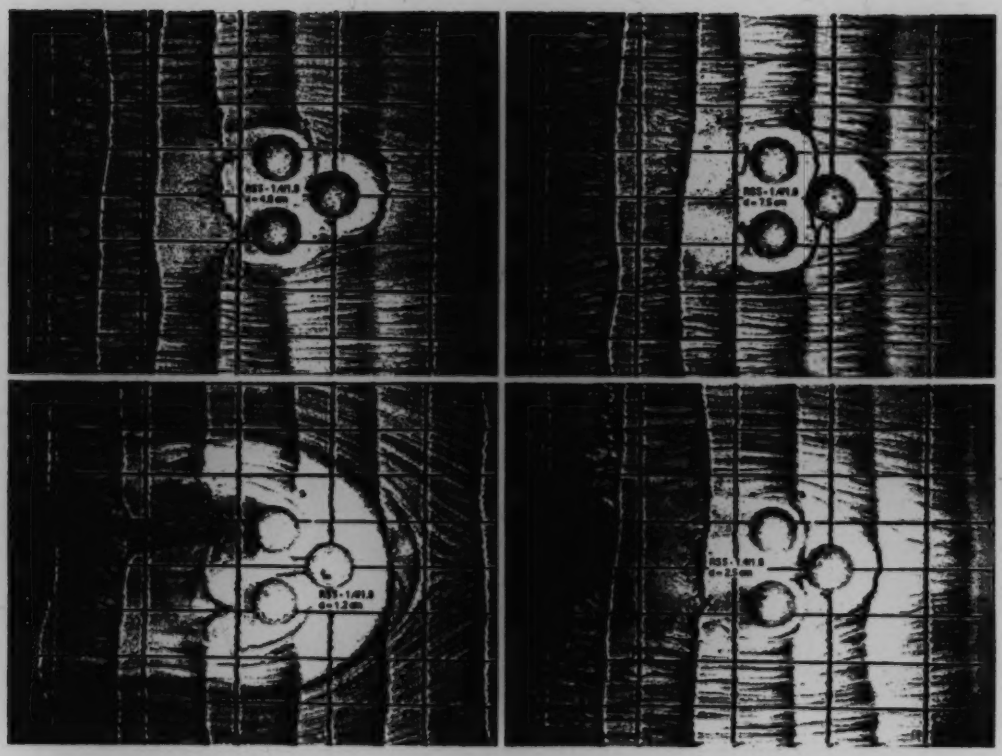

LABELLING NOTATION

RSD-S/S'
d=depth of flow (cm)

RS - Bed configuration (Rigid Smooth)

D - Diameter of obstacle

S and S' are scalars of the length scale D

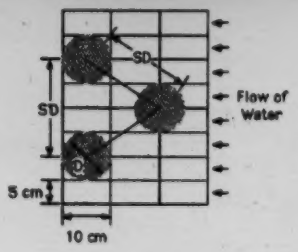

PICTURE ARRANGEMENT

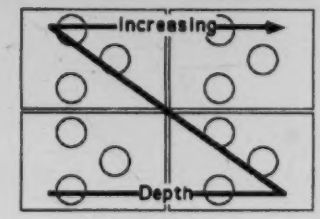

Figure B10. Composite BSP, D = 5 cm, S/S' = 1.4/1.6

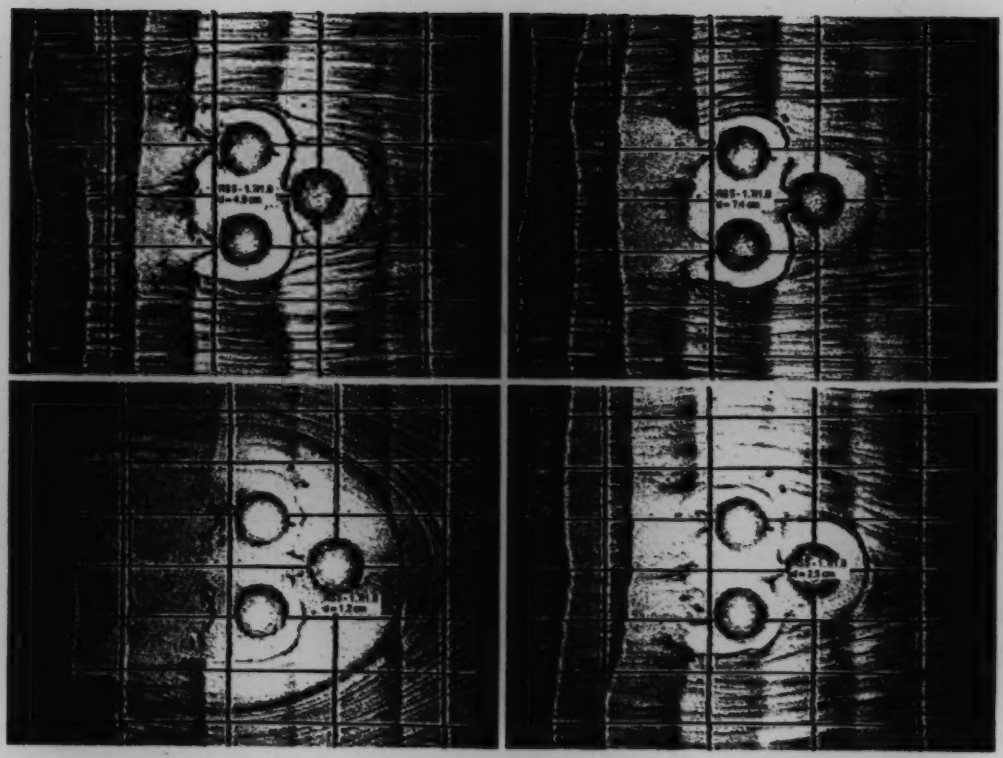

LABELLING NOTATION

RSD-S/S'
d=depth of flow (cm)

RS – Bed configuration (Rigid Smooth)

D – Diameter of obstacle

S and S' are scalars of the length scale D

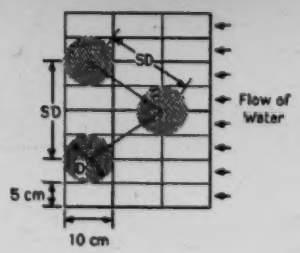

PICTURE ARRANGEMENT .

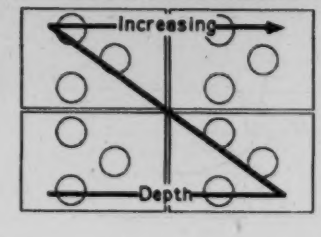

Figure B11. Composite BSP, D = 5 cm, S/S' = 1.7/1.8

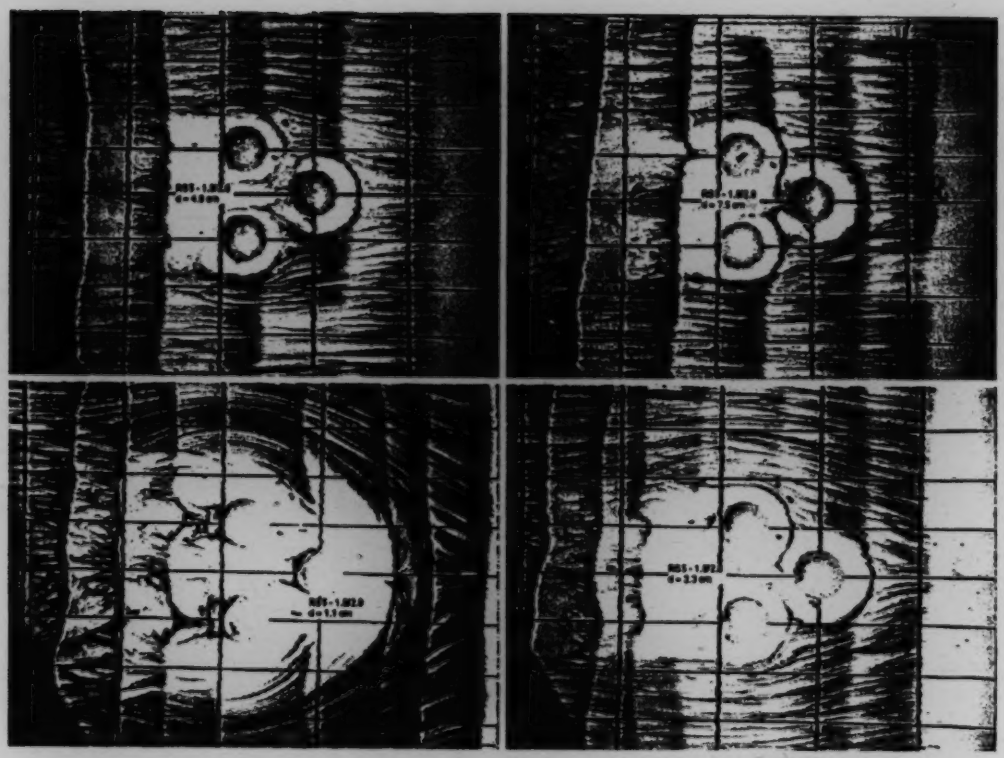

LABELLING NOTATION

RSD-S/S'
d=depth of flow (cm)

RS - Bed configuration (Rigid Smooth)

D - Diameter of obstacle

S and S' are scalars of the length scale D

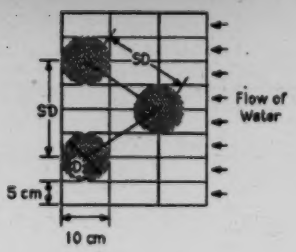

PICTURE ARRANGEMENT

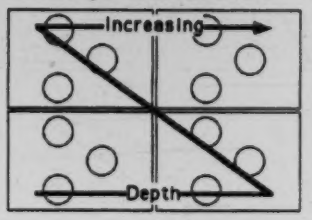

Figure B12. Composite BSP, D = 5 cm, S/S' = 1.8/2.0

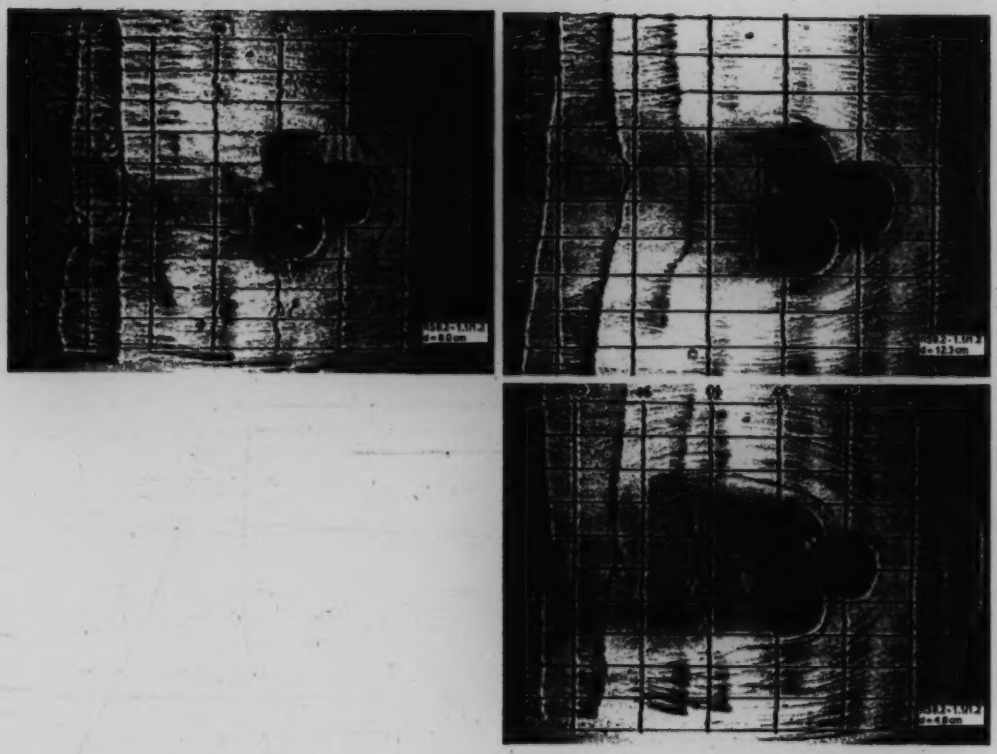

LABELLING NOTATION

RSD-S/S'
d=depth of flow (cm)

RS - Bed configuration (Rigid Smooth)

D - Diameter of obstacle

S and S' are scalers of the length scale D

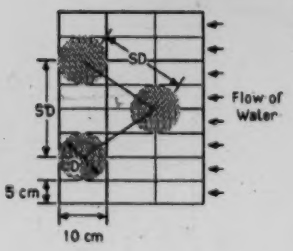

PICTURE ARRANGEMENT

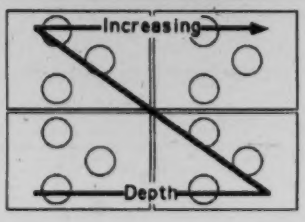

Figure B13. Composite BSP, D = 8.2 cm, S/S' = 1.1/1.2

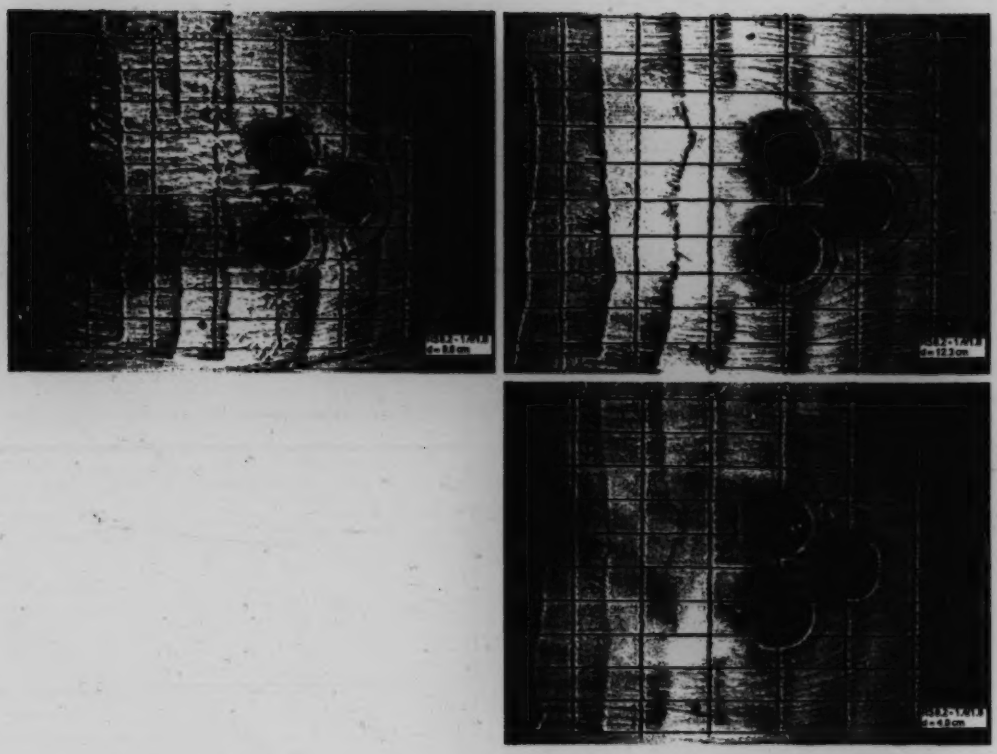

LABELLING NOTATION

RSD-S/S'
d=depth of flow (cm)

RS - Bed configuration (Rigid Smooth)

D - Diameter of obstacle

S and S' are scalers of the length scale D

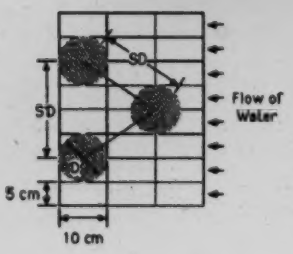

PICTURE ARRANGEMENT

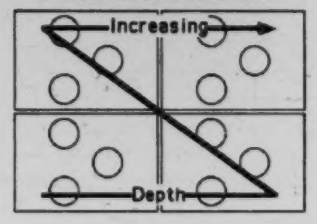

Figure B14. Composite BSP, D = 8.2 cm, S/S' = 1.4/1.6

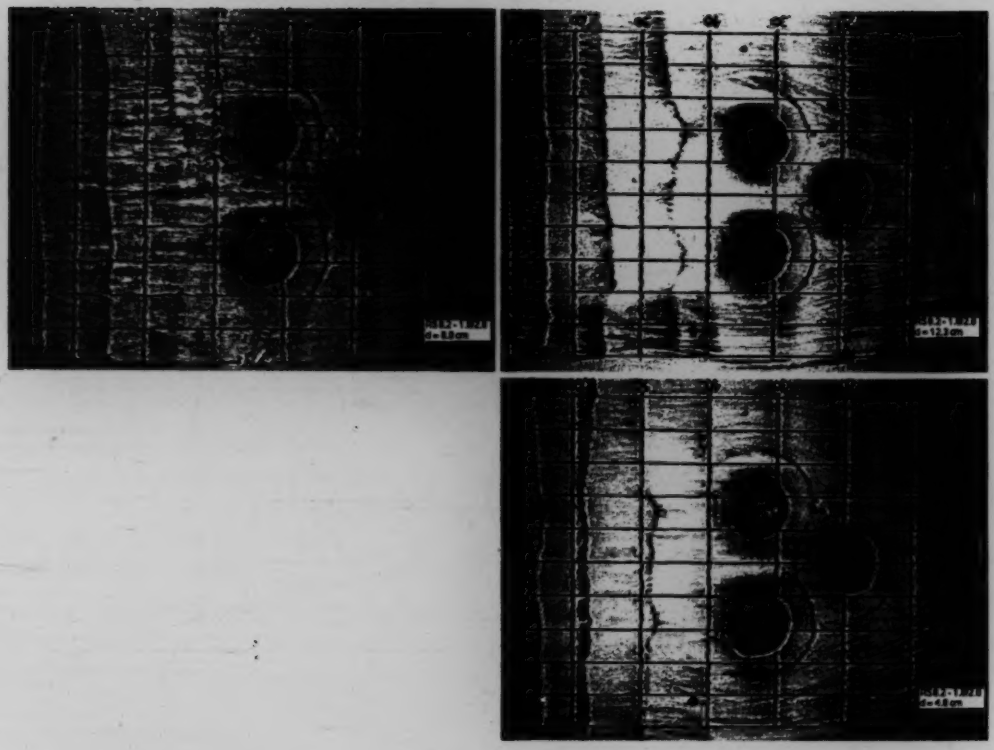

LABELLING NOTATION

RSD-S/S'
d=depth of flow (cm)

RS - Bed configuration (Rigid Smooth)

D - Diameter of obstacle

S and S' are scalars of the length scale D

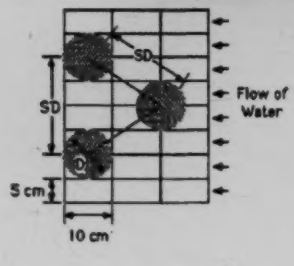

PICTURE ARRANGEMENT

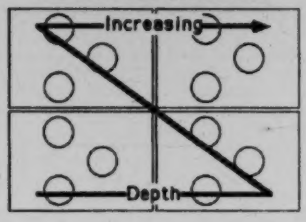

Figure B15. Composite BSP, D = 8.2 cm, S/S' = 1.8/2.0